ACS NANO

www.acsnano.org

ARTICLE

Targeted mRNA Nanoparticles Ameliorate Blood–Brain Barrier Disruption Postischemic Stroke by Modulating Microglia Polarization

Mingzhu Gao, Yan Li, William Ho, Chen Chen, Qijing Chen, Fengshi Li, Maoping Tang, Qiuyue Fan, Jieqing Wan, Weifeng Yu, Xiaoyang Xu, Peiying Li,* and Xue-Qing Zhang*

Cite This: *ACS Nano* 2024, 18, 3260–3275

Read Online

ACCESS | Metrics & More | Article Recommendations | Supporting Information

ABSTRACT: **The ischemic stroke is a major global health concern, with high mortality and disability rates. Unfortunately, there is a dearth of effective clinical interventions for managing poststroke neuroinflammation and blood–brain barrier (BBB) disruption that are crucial for the brain injury evolving and neurological deficits. By leveraging the pathological progression of an ischemic stroke, we developed an M2 microglia-targeting lipid nanoparticle (termed MLNP) approach that can selectively deliver mRNA encoding phenotype-switching interleukin-10 (m*IL-10*) to the ischemic brain, creating a beneficial feedback loop that drives microglial polarization toward the protective M2 phenotypes and augments the homing of m*IL-10*-loaded MLNPs (m*IL-10*@MLNPs) to ischemic regions. In a transient middle cerebral artery occlusion (MCAO) mouse model of an ischemic stroke, our findings demonstrate that intravenously injected m*IL-10*@MLNPs induce IL-10 production and enhance the M2 polarization of microglia. The resulting positive loop reinforces the resolution of neuroinflammation, restores the impaired BBB, and prevents neuronal apoptosis after stroke. Using a permanent distal MCAO mouse model of an ischemic stroke, the neuroprotective effects of m*IL-10*@MLNPs have been further validated by the attenuation of the sensorimotor and cognitive neurological deficits. Furthermore, the developed mRNA-based targeted therapy has great potential to extend the therapeutic time window at least up to 72 h poststroke. This study depicts a simple and versatile LNP platform for selective delivery of mRNA therapeutics to cerebral lesions, showcasing a promising approach for addressing an ischemic stroke and associated brain conditions.**

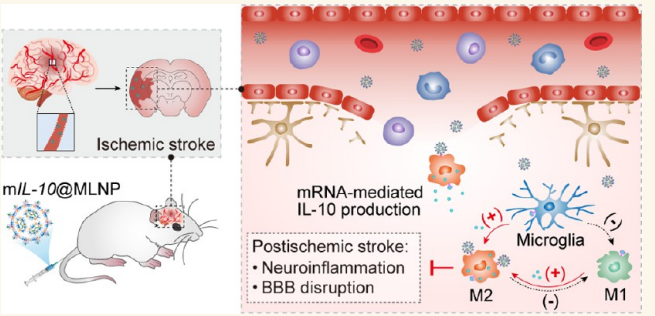

KEYWORDS: *ischemic stroke, lipid nanoparticle, targeted delivery, mRNA, phenotypic switch*

INTRODUCTION

The ischemic stroke is the second leading cause of adult death and disability worldwide, resulting in 5.9 million deaths annually.[1] The high mortality and long-term disability rates have made the ischemic stroke one of the most serious public health concerns.[2] Although the current clinical treatment options of recombinant tissue plasminogen activator (rtPA) and endovascular thrombectomy (EVT) benefit some stroke patients in 4.5 and 24 h postsymptom onset,[3] the clinical issues of blood–brain barrier (BBB) disruption and secondary neuronal damage poststroke remain inadequately addressed, potentially increasing the risk of hemorrhagic transformation and catastrophic outcomes.[4−6] As a result, there is a critical demand to develop therapeutic strategies capable of effectively mitigating neuroinflammation and preserving the integrity of BBB to protect the neurological functions poststroke.

Emerging evidence has revealed that neuroimmune responses are integral parts of the ischemic stroke, which are intimately involved in all stages of the pathological process from acute brain damage to extended tissue damage.[7] In the early stroke phase, the innate immune effector cells of the central nervous system (CNS), i.e., the microglia, are the primary cells that quickly respond (<1 h) to the ischemic insult and boost restorative processes after acute cerebral injury through eliminating cellular debris and producing anti-

Received: October 9, 2023
Revised: January 2, 2024
Accepted: January 9, 2024
Published: January 16, 2024

https://doi.org/10.1021/acsnano.3c09817
ACS Nano 2024, 18, 3260–3275

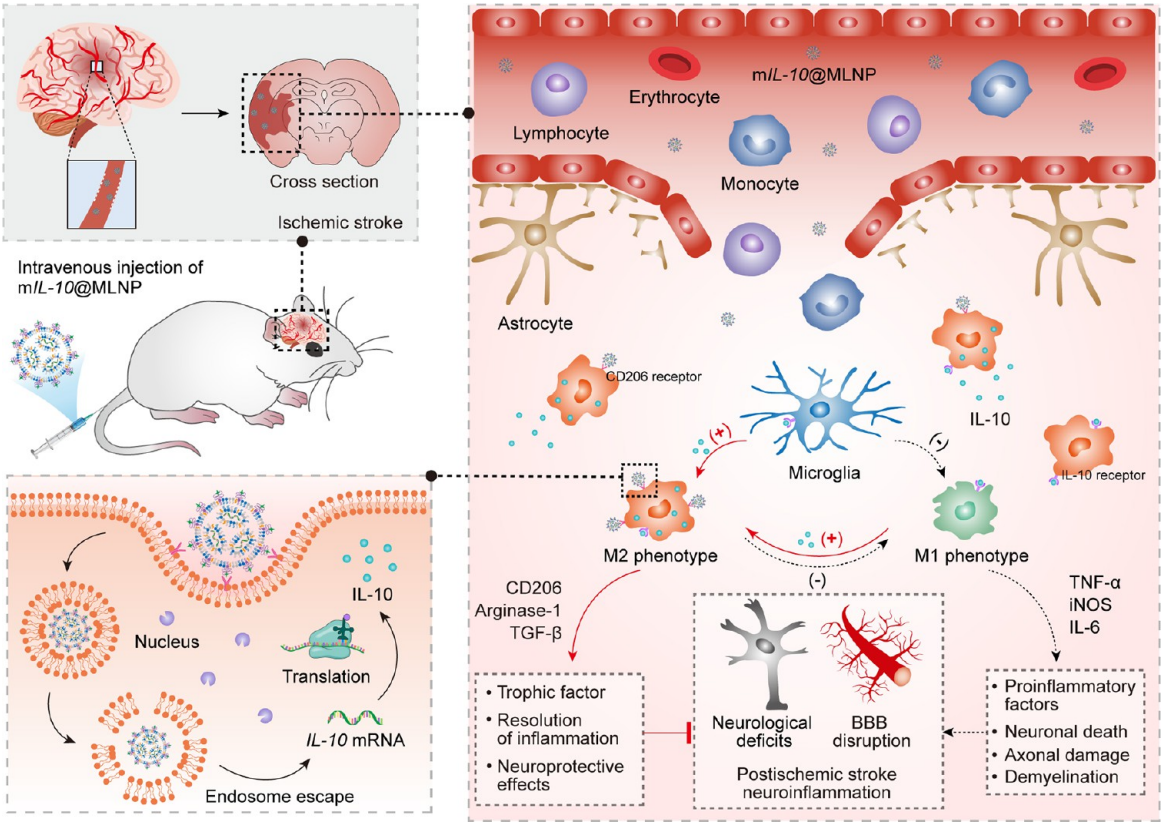

Figure 1. Schematic illustration of LNP-mediated delivery of m*IL-10* to M2 microglia in cerebral ischemic regions for poststroke neurological repair. m*IL-10*@MLNPs can cross the leaky BBB and selectively target M2-polarized microglia located in ischemic brain regions via mannose receptor-mediated interactions. Following internalization, MLNPs are able to escape from endosomes and release therapeutic mRNA into the cytoplasm, inducing the production of IL-10. The secreted IL-10 drives the polarization of microglia toward M2 phenotypes, which in turn facilitates the homing of MLNPs into the ischemic brain lesions. The resulting positive feedback loop augments the anti-inflammatory effects of m*IL-10*@MLNPs, elevating trophic factors like CD206, arginase-1 (Arg-1), and transforming growth factor *β* (TGF-*β*), while reducing the expression of pro-inflammatory cytokines, including tumor necrosis factor *α* (TNF-*α*), inducible nitric oxide synthase (iNOS), and interleukin-6 (IL-6). Moreover, the elevated levels of IL-10 ameliorate neuronal death, BBB damage, and neurological deficits, resulting in tissue repair and function recovery.

inflammatory mediators at the lesion sites.[8] Upon pathological progression, the early recruited protective microglia undergo a rapid phenotypic switch from M2-dominant to M1-dominant, accompanied by an upregulation of inflammatory substances such as cytokines, chemokines, and reactive oxygen species (ROS); these events then lead to the progression of neuroinflammation, BBB breakdown, and neuronal death.[9] This pathological process highlights the phenotype-switching molecules that drive the M1 to M2 shift as attractive therapeutic targets to mitigate neuroinflammation and BBB disruption following ischemic brain injury.

IL-10, a robust anti-inflammatory cytokine, can promote M2 polarization of microglia through Janus kinase-STAT pathways,[10] thereby resolving the neuroinflammatory microenvironment, protecting against BBB disruption, and restoring neurological function following an ischemic stroke.[11,12] Despite its promising neuroprotective role, the clinical translation of IL-10 has been limited due to its brief plasma half-life (approximately 3 min) and the risks of immunosuppression and infection associated with systemic administration at high doses.[13,14] It is thus imperative to develop strategies that enable local expression of bioactive IL-10 in the ischemic brain, driving microglial polarization toward M2 phenotypes and resolving the neuroinflammation that exacerbates brain injury and BBB disruption following a cerebral ischemic stroke.

Recently, mRNA has rapidly emerged as a versatile therapeutic for preventing and managing various diseases, due to its flexibility, scalability, and the ability to produce any protein of interest.[15−17] It is essential to develop nanocarriers that facilitate the delivery of mRNA therapeutics to specific organs and cell types, unlocking the full potential of mRNA-based therapy.[18−20] Despite advances in mRNA delivery, there remains a lack of targeted delivery vehicles, particularly those that allow for the selective delivery of therapeutic mRNA to ischemic lesions in the brain microenvironment, which have yet to be explored.

To address this unmet need, we developed M2 microglia-targeting nanoparticles (NPs) capable of specifically delivering mRNA encoding phenotype-switching IL-10 that shifts microglia toward M2 phenotypes, resulting in a beneficial feedback loop that facilitates the homing of NPs to the ischemic brain and improves poststroke tissue repair and functional recovery (Figure 1). To bring this design to fruition, we selected a mannose moiety with high affinity for M2 microglia as the building block to synthesize mannose-tethered DMG-PEG (DMG-PEG-Mannose), which was then combined with our previously developed amino-ionizable lipid AA3-Dlin to construct MLNPs. These MLNPs can recognize the CD206 receptor highly expressed on the surface of M2 microglia, thus facilitating the delivery of m*IL-10* to ischemic regions of brain.

https://doi.org/10.1021/acsnano.3c09817
ACS Nano 2024, 18, 3260−3275

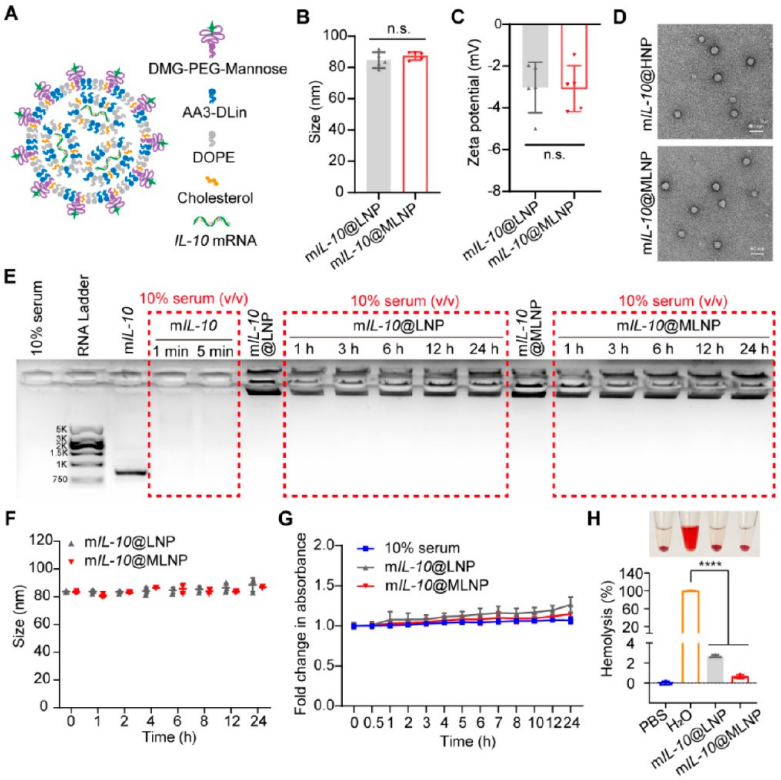

Figure 2. Preparation and characterization of m*IL-10*-encapsulated LNPs. (A) Schematic of targeted m*IL-10*@MLNPs. (B and C) Average particle size (B) and zeta potential (C) measurements of m*IL-10*@LNPs and m*IL-10*@MLNPs (n = 5). (D) TEM images of m*IL-10*-loaded LNPs. (E) Durability of unprotected mRNA and LNP-encapsulated mRNA against serum-induced degradation. (F and G) Size (F) and turbidity (G) of m*IL-10*-loaded LNPs in 10% serum condition at 37 °C for up to 24 h (n = 3). (H) Hemolytic ratio of m*IL-10*-loaded LNPs (n = 3). All data are shown as means ± SD, and statistical significance was determined using one-way ANOVA (**P < 0.0001). n.s., not significant.**

In a transient MCAO (tMCAO) mouse model of an ischemic stroke, our findings demonstrated that intravenously injected m*IL-10*@MLNPs induced the production of IL-10 in infarct areas, which promoted the M2 polarization of microglia in the ischemic brain and subsequently enhanced NP accumulation. This resultant positive feedback loop amplified the m*IL-10*@MLNP-mediated anti-inflammatory response, thereby enhancing the BBB integrity and reducing neuronal death after stroke. We further investigated the therapeutic efficacy of m*IL-10*-loaded MLNPs in a distal MCAO (dMCAO) mouse model, which showed a significant reduction in BBB disruption and the successful alleviation of sensorimotor and cognitive neurological dysfunction. This work presents a proof-of-concept for the design and preclinical assessment of targeted LNPs that can selectively deliver inflammation-resolving m*IL-10* to cerebral ischemic lesions, offering potential therapeutic benefits for stroke patients with a long therapeutic window up to at least 72 h poststroke.

RESULTS

Synthesis and Characterization of mRNA LNPs. As shown in Figure 2A, MLNPs were constructed through self-assembly of AA3-ionizable lipid AA3-Dlin that we reported previously, mannose conjugated DMG-PEG, DOPE, and cholesterol using a microfluidic method. AA3-Dlin was rationally designed to consist of tertiary amine head groups from piperazine, carbon chains from unsaturated linolenic acids, and biodegradable ester linkers and was synthesized through an enzyme-assisted one-step esterification (Figures S1 and S2). Our previous results demonstrated that AA3-Dlin could effectively condense mRNA via electrostatic interactions and facilitate its endosomal escape after cellular endocytosis, resulting in superior mRNA translation efficiency both in vitro and in vivo.[21] To endow LNPs with the ability to target M2 microglia, mannose moieties capable of strongly binding to the CD206 receptor were covalently coupled to the end of the PEG-lipid via an amide bond (Figure S3). We synthesized m*IL-10* using an in vitro transcription method as described previously,[22] and characterized the physicochemical property of LNPs incorporating m*IL-10*. Dynamic light scattering (DLS) results show that the targeted m*IL-10*@MLNPs have an average size of ∼87 nm and a nearly neutral surface potential of ∼−3 mV, akin to the nontargeted m*IL-10*@LNPs (Figure 2B,C). This indicates that the incorporation of mannose moieties has a negligible effect on the size and zeta potential of LNPs. Transmission electron microscopy (TEM) images exhibited the uniform and spherical structure of LNPs (Figure 2D). mRNA encapsulated within LNPs exhibited excellent stability when exposed to 10% fetal bovine serum (FBS) for at least 24 h but rapidly degraded in its free form (Figure 2E). We then incubated LNPs in the presence of serum at 37 °C to mimic physiological conditions and observed no significant change in particle size over 24 h (Figure 2F). Additionally, turbidity measurements confirmed that there was no serum-induced aggregation of LNPs (Figure 2G). Both targeted MLNPs and nontargeted LNPs demonstrated good blood compatibility, as neither of them showed >5% hemolysis ratio (Figure 2H). These data indicate that the

https://doi.org/10.1021/acsnano.3c09817
ACS Nano 2024, 18, 3260−3275

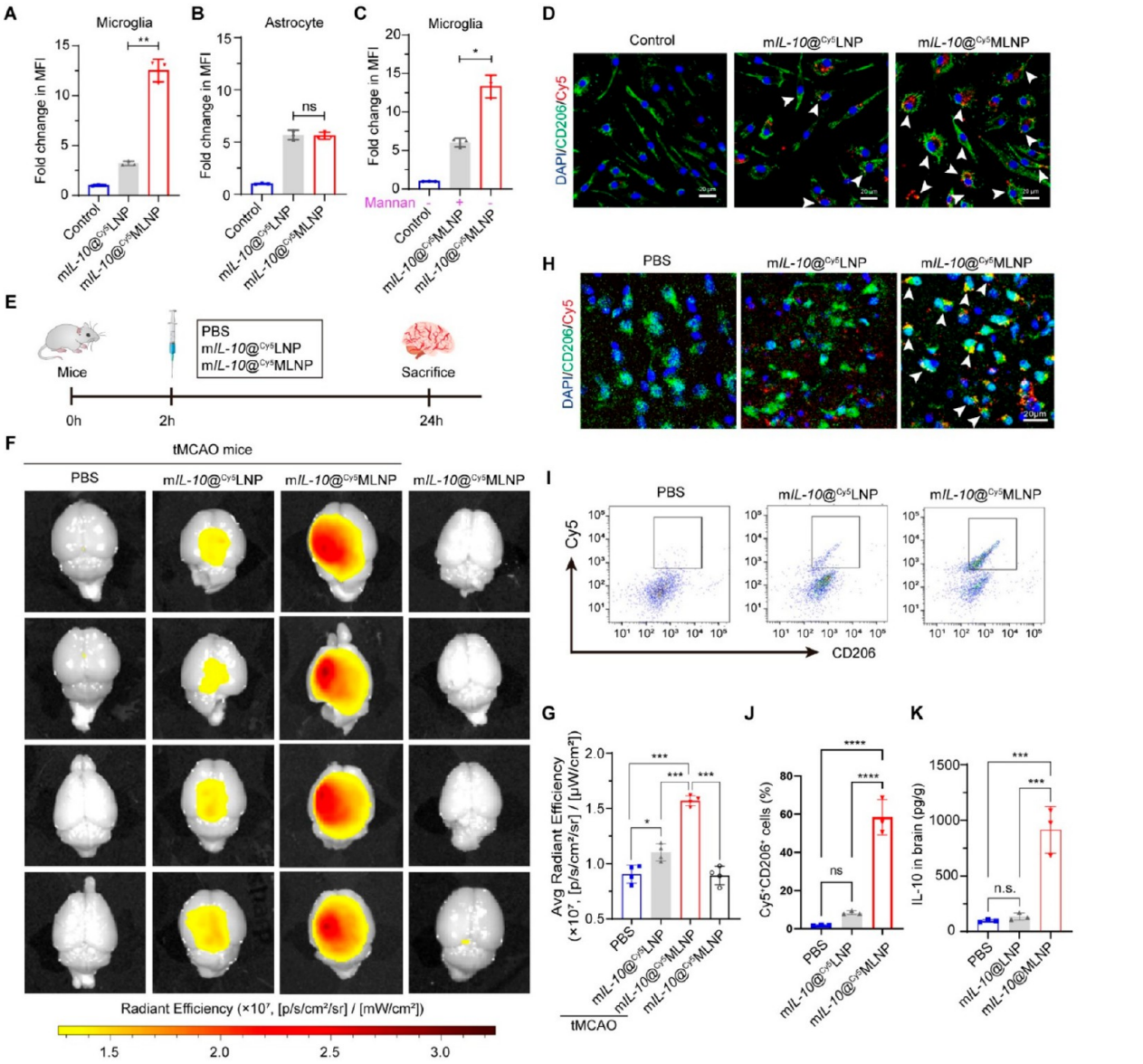

Figure 3. Cellular uptake of m*IL-10*-loaded LNPs in vitro and their targeting ability in cerebral ischemic regions of tMCAO mice after intravenous administration. (A to C) Fold change in mean fluorescence intensity (MFI) of IL-4-induced microglia (A and C) or astrocyte (B) incubated with ^{Cy5}LNPs for 4 h by flow cytometry analysis (n = 3). IL-4-stimulated microglia were pretreated with mannan and subsequently incubated with m*IL-10*@^{Cy5}MLNPs for 4 h (C). (D) CLSM images of IL-4-stimulated microglia incubated with ^{Cy5}LNPs (red) for 4 h. CD206 immunostaining (green) was applied to microglia, and DAPI (blue) was used for nuclei staining. White arrows pinpoint the colocalization of CD206 with ^{Cy5}LNPs. Scale bar: 20 μm. (E) Injection schedule of LNPs in tMCAO mice. (F) IVIS imaging of the brains in healthy mice or tMCAO mice 24 h postintravenous administration of PBS, m*IL-10*@^{Cy5}LNPs, or m*IL-10*@^{Cy5}MLNPs. (G) Quantitative analysis of fluorescence signal in brain by Living Image 4.5 software (n = 4). (H) Immunofluorescence analysis of ^{Cy5}LNPs (red) and CD206$^+$ microglia (green) colocalization in the tissue sections of cerebral hemispheres with ischemic lesions. White arrows pinpoint the colocalization of CD206 with ^{Cy5}LNPs. Scale bar: 20 μm. (I and J) Representative histogram (I) and quantification (J) of ^{Cy5}LNP-containing CD206$^+$ microglia isolated from cerebral ischemic hemispheres of tMCAO mice (n = 3). (K) ELISA analysis of IL-10 in cerebral ischemic hemispheres obtained from tMCAO mice receiving the indicated treatments (n = 3). The data are presented as mean ± SD, and one-way ANOVA was used to determine statistical significance (*P < 0.05, **P < 0.01, ***P < 0.001, and **** P < 0.0001). n.s., not significant.

developed MLNPs possess a stable nanostructure capable of protecting the enclosed mRNA from degradation.

MLNPs Target M2-Polarized Microglia In Vitro and In Vivo. We then formulated m*IL-10*-loaded LNPs using Cy5-labeled cholesterol and examined cellular internalization of the resultant ^{Cy5}LNPs by M2-polarized microglia stimulated by Interleukin-4 (IL-4). Flow cytometry results showed that the incorporation of mannose moieties led to an increased uptake of m*IL-10*@^{Cy5}MLNP by M2 microglia (Figure 3A). In contrast, this enhanced uptake of m*IL-10*@^{Cy5}MLNPs was not observed in astrocytes that do not overexpress CD206 (Figure 3B). Additionally, treatment with mannan (a CD206 antagonist) significantly decreased the uptake of m*IL-10*@^{Cy5}MLNP by M2 microglia (Figure 3C). Confocal laser scanning microscopy (CLSM) images demonstrated a higher degree of colocalization between m*IL-10*@^{Cy5}MLNPs and

https://doi.org/10.1021/acsnano.3c09817
ACS Nano 2024, 18, 3260−3275

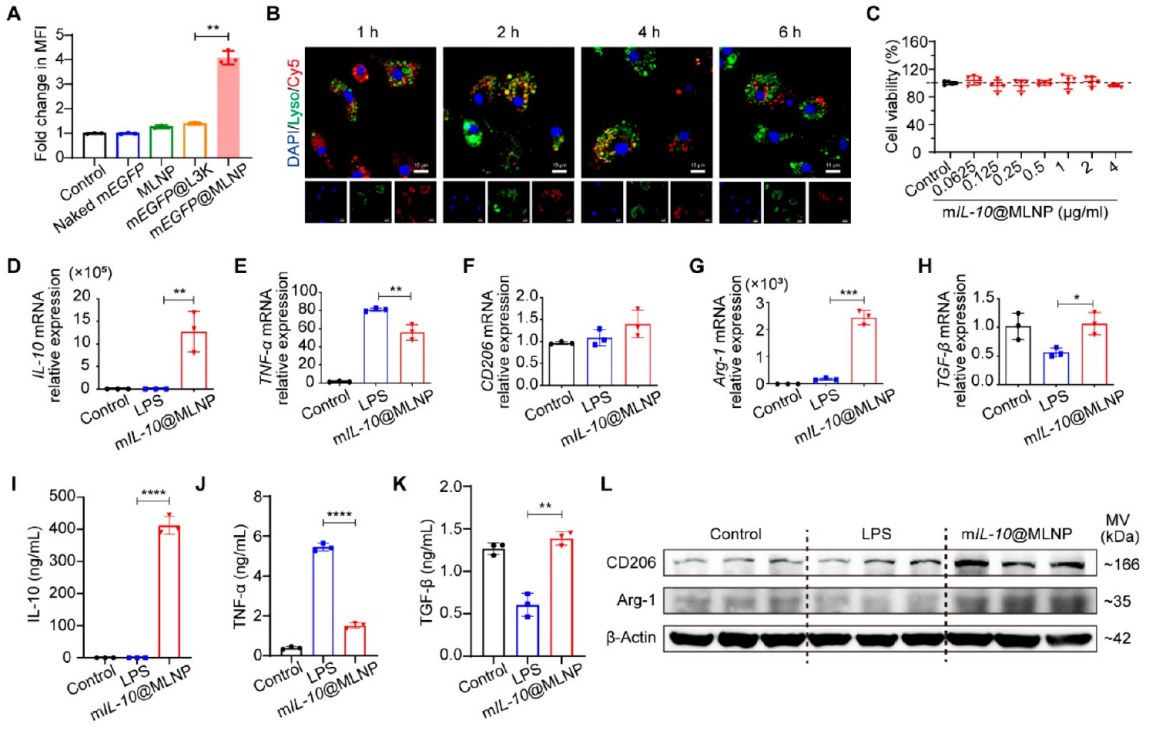

Figure 4. Assessment of m*IL-10*@MLNPs for transfection efficacy and anti-inflammatory properties in vitro. (A) Flow cytometry determination of transfection efficacy in microglia (n = 3). (B) CLSM images of microglia after incubation with ^{Cy5}mRNA@MLNPs (red) for 1, 2, 4, and 6 h. The Hoechst 33342 dye (blue) was used to label the nuclei, while LysoTracker Green (green) was employed to stain endosomes. Scale bar: 10 μm. (C) Cell viability assay of microglia after incubation with m*IL-10*@MLNPs across a range of mRNA concentrations (0.0625, 0.125, 0.25, 0.50, 1, 2, or 4 μg/mL) for 24 h (n = 5). (D to H) Real-time quantitative reverse transcription PCR (RT-qPCR) analysis for mRNA expression of *IL-10* (D), *TNF-α* (E), *CD206* (F), *Arg-1* (G), and *TGF-β* (H) in primary microglia that have been stimulated by LPS for 4 h followed by treatment with m*IL-10*@MLNPs for 24 h (n = 3). (I to K) ELISA analysis for IL-10 (I), TNF-α (J), and TGF-β (K) levels in primary microglia stimulated by LPS and subsequent m*IL-10*@MLNPs treatment (n = 3). (L) Western blotting of CD206 and Arg-1 in LPS-induced primary microglia treated with m*IL-10*@MLNPs. Utilization of β-Actin was a reference standard (n = 3). The data are depicted as means ± SD, and statistical significance was evaluated through one-way ANOVA (*P < 0.05, **P < 0.01, ***P < 0.001, and **** P < 0.0001). n.s., not significant.

CD206 expressed on the M2 microglia surface compared to nontargeted m*IL-10*@^{Cy5}LNPs (Figure 3D). Moreover, both flow cytometry results and CLSM images indicated time- and dose-dependent internalization of m*IL-10*@^{Cy5}MLNPs by microglia (Figure S4). These results suggest that the enhanced uptake of MLNP by M2 microglia is predominantly dependent on mannose receptor-mediated endocytosis.

We then established a tMCAO model in C57BL/6 male mice to evaluate the in vivo targeting ability of the mRNA LNPs. Mice were intravenously injected with ^{Cy5}LNPs or ^{Cy5}MLNPs encapsulating an equivalent dose of m*IL-10* 2 h following tMCAO (Figure 3E). In vivo imaging system (IVIS) images of brains showed that the incorporation of mannose moieties significantly increased the level of cerebral accumulation of m*IL-10*@^{Cy5}MLNPs (Figure 3F,G). Approximately 1.24% of targeted m*IL-10*@MLNPs accumulated in the brains of tMCAO mice, a significantly higher rate compared to the localization of nontargeted m*IL-10*@LNPs (~0.17%) in the brains (Figure S5). Immunofluorescence images of brain sections showed abundant colocalization of m*IL-10*@^{Cy5}MLNPs with CD206^{+} microglia, suggesting that the majority of microglia within the early ischemic brain polarize into the M2 phenotypes and express a high level of CD206 (Figure 3H). Flow cytometry analysis revealed that the uptake of m*IL-10*@^{Cy5}MLNPs by CD206^{+} cerebral microglia was ~7.5-fold higher than that of the nontargeted m*IL-10*@^{Cy5}LNPs (Figure 3I,J). IL-10 levels in the ischemic hemisphere of brain tissues were detected by ELISA. The results showed a notable increase in IL-10 expression within the cerebral ischemic hemispheres of mice receiving m*IL-10*@MLNP treatment compared to those receiving PBS or m*IL-10*@LNP treatment (Figure 3K). Consistent with previous studies,[23] the accumulation of small-sized LNPs or MLNPs was also observed in the livers and kidneys that are responsible for drug metabolism and elimination following systemic administration (Figure S5). Taken together, our findings reveal that MLNPs can specifically target M2 microglia via ligand−receptor interactions, thereby facilitating the homing of mRNA-loaded MLNPs to cerebral ischemic regions.

In Vitro Assessment of MLNP-Mediated mRNA Transfection and Anti-inflammatory Effects. It is notoriously difficult to transfect microglia to express specific proteins due to their high level of differentiation and resistance to foreign nucleic acid.[24] Here, we evaluate the transfection efficiency of mRNA MLNPs in microglia using enhanced green fluorescent protein mRNA (m*EGFP*) as a model mRNA. Flow cytometry analysis revealed that microglia treated with m*EGFP*@MLNPs had a higher MFI than those treated with the commercial transfection agent Lipofectamine 3000 (L3K) (Figure 4A). Next, MLNPs loaded with Cy5-labled mRNA (termed ^{Cy5}mRNA@MLNPs) were incubated with microglia for 1, 2, 4, or 6 h (Figure 4B). CLSM images showed that most

https://doi.org/10.1021/acsnano.3c09817
ACS Nano 2024, 18, 3260−3275

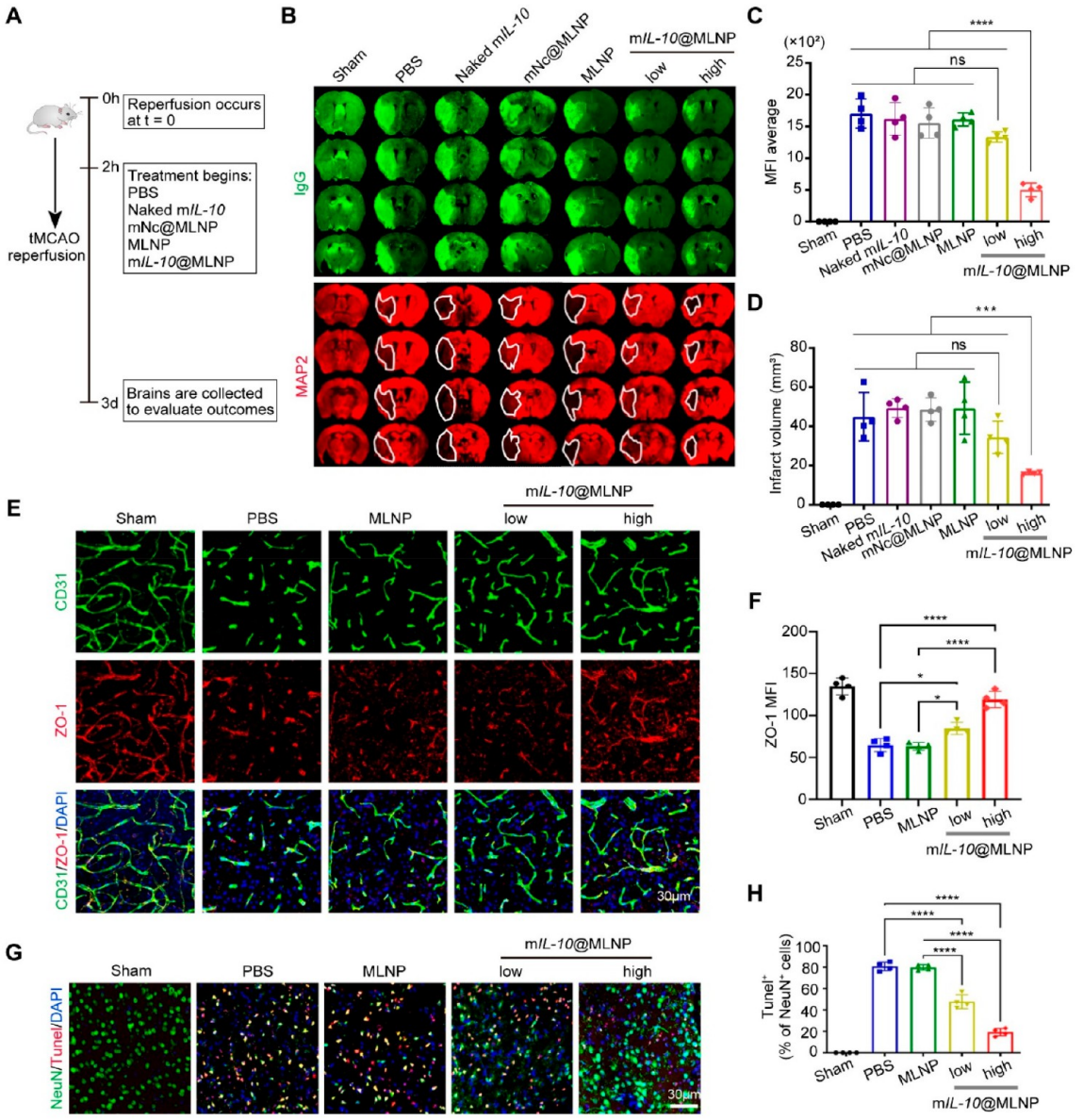

Figure 5. Therapeutic validation of m*IL-10*@MLNPs on BBB integrity and neuronal survival in tMCAO mice. (A) Schematic illustration of the treatment regimen for tMCAO mice with an established ischemic stroke. (B) Representative immunofluorescence images of endogenous IgG extravasation and MAP2 in brain sections obtained from sham-operated mice or tMCAO mice treated with PBS, Naked m*IL-10*, mNc@MLNPs, MLNPs, or m*IL-10*@MLNPs (n = 4). White solid lines indicate the infarct border. (C and D) Quantification of IgG MFI (C) and infarct volume (D) in brain sections obtained from sham-operated mice or tMCAO mice receiving the indicated treatments (n = 4). (E and F) Representative CLSM images (F) and MFI quantification (G) of ZO-1 (red) in brain sections from the indicated groups (n = 4). Nuclei were stained with DAPI (blue) and endothelial cells were immunestained with CD31 (green). Scare bar: 30 μm. (G) Representative CLSM images of TUNEL (red) and NeuN (green) in brain sections from the indicated groups. The cellular nuclei were labeled using DAPI (blue). Scare bar: 30 μm. (H) Percentage of apoptotic neurons relative to the total number of neurons shown in (G) (n = 4). All data are shown as means ± SD, and statistical significance was determined using one-way ANOVA (*P < 0.05, ***P < 0.001, and **** P < 0.0001). n.s., not significant.

^{Cy5}mRNA@MLNPs were internalized by microglia after 1 h incubation and colocalized with endosome upon 2 h of incubation. After incubation for 4 h, a considerable amount of ^{Cy5}mRNA-loaded MLNPs had escaped from endosomes, and nearly all of the MLNPs had fully diffused into the cytoplasm within 6 h. These results suggest that MLNPs facilitate rapid mRNA escape from endosomes and its subsequent release into the cytoplasm, likely accounting for the effective transfection observed in microglia. Notably, no reduction in the viability of cells was observed upon MLNP treatment at a high concentration of up to 4 μg/mL of mRNA, indicating excellent biocompatibility of m*IL-10*@MLNPs (Figure 4C and Figure S6).

We conducted transfection experiments in isolated primary microglia and BV2 cells to evaluate the efficacy of IL-10 translation and the anti-inflammatory effects mediated by m*IL-10*@MLNPs. The results showed that treatment with m*IL-10*@MLNPs markedly elevated expression levels of IL-10

https://doi.org/10.1021/acsnano.3c09817
ACS Nano 2024, 18, 3260−3275

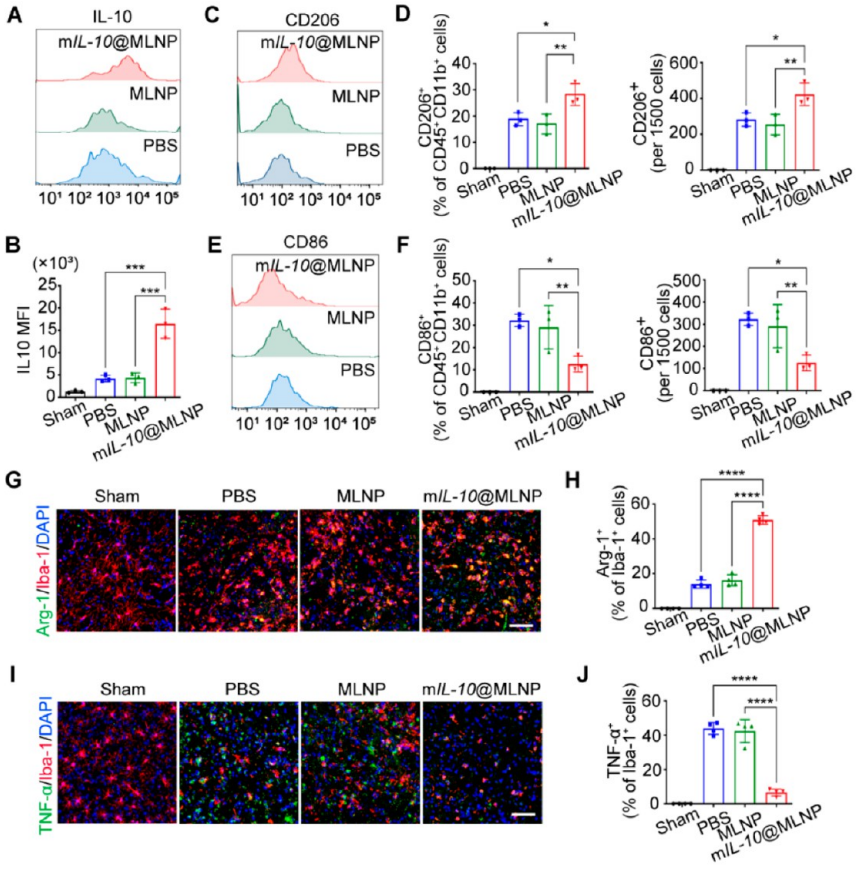

Figure 6. Effects of m*IL-10*@MLNP treatment on phenotypic shifts of microglia and resolution of neuroinflammation in tMCAO mice. (A and B) Representative histogram (A) and quantification (B) of IL-10 expression in $CD45^+CD11b^+$ microglia isolated from the cerebral ischemic hemispheres from the indicated treatment groups (n = 3). (C and D) Representative histogram (C) and quantification (D) of $CD206^+$ microglia isolated from the cerebral ischemic hemispheres from the indicated treat ment groups (n = 3). (E and F) Representative histogram (E) and quantification (F) of $CD86^+$ microglia isolated from the cerebral ischemic hemispheres from the indicated treatment groups (n = 3). (G) Representative CLSM images of Arg-1 (green) in the brain sections obtained from the cerebral hemispheres with ischemic regions from the indicated treatment groups. Nuclei were stained with DAPI (blue), and Microglia were immunostained with Iba-1 (red). Scare bar: 20 μm. (H) Quantification of $Arg\text{-}1^+$ microglia shown in (G) (n = 4). (I and J) Representative CLSM images (I) and quantitative analysis (J) of TNF-α (green) and Iba-1 (red) in the brain sections obtained from the cerebral hemispheres with ischemic regions (n = 4). Nuclei were stained with DAPI (blue). Scare bar: 20 μm. The data are presented as means ± SD, and statistical significance was assessed through one-way ANOVA, denoted by *P < 0.05, **P < 0.01, ***P < 0.001, and **** P < 0.0001.

(Figure 4D,I and Figure S7). We then investigated whether m*IL-10*@MLNPs could modulate the lipopolysaccharide (LPS)-induced inflammatory response in microglia in the following experiments. LPS stimulation elevated the production of TNF-α, a key pro-inflammatory cytokine, within microglia. m*IL-10*@MLNP treatment substantially suppressed TNF-α production and elevated CD206 expression at both mRNA and protein levels in LPS-stimulated microglia, which is likely a result of the effective production of bioactive IL-10 via MLNP-mediated mRNA delivery (Figure 4E,F,J,L). This potent anti-inflammatory effect was further confirmed by the reduced expression of iNOS and IL-6 in LPS-stimulated BV2 cells following treatment with m*IL-10*@MLNP (Figure S7). Additionally, MLNP treatment significantly enhanced the production of protective and trophic factors Arg-1 and TGF-β in LPS-stimulated microglia, indicating a microglial shift toward anti-inflammatory M2 phenotypes (Figure 4G,H,K,L and Figure S7).

m*IL-10*@MLNP Treatment Ameliorates BBB Damage and Neuronal Death in the tMCAO Mouse Model. Next, we explored the therapeutic outcomes of MLNPs for the selective delivery of m*IL-10* to cerebral M2 microglia within a tMCAO mouse model. tMCAO mice were intravenously injected with different treatments 2 h after reperfusion. PBS, Naked m*IL-10*, Noncoding mRNA-loaded MLNPs (termed mNc@MLNPs), and blank MLNPs were administrated as control treatments. Brains were collected 3 days after injection to evaluate therapeutic outcomes (Figure 5A). To assess ischemia-reperfusion injury related BBB disruption after tMCAO, brain sections were stained for endogenous plasma IgG, and the resultant green fluorescence region indicated extravasation of blood components into the brain parenchyma. m*IL-10*@MLNP treatment, particularly at a dosage of 0.6 mg/kg of mRNA, significantly ameliorated BBB disruption, as evidenced by a reduction in the green fluorescence signal corresponding to IgG (Figure 5B,C). Additionally, microtubule-associated protein-2 (MAP-2) staining results demonstrated that treatment with m*IL-10*@MLNPs at both low and high doses exhibited a reduction in mean infarct volumes compared to the control groups, from 44.92 ± 12.32 mm^3 (PBS control), 49.38 ± 4.79 mm^3 (Naked m*IL-10* control), 48.54 ± 6.00 mm^3 (mNC@MLNP control), and 49.25 ±

https://doi.org/10.1021/acsnano.3c09817
ACS Nano 2024, 18, 3260−3275

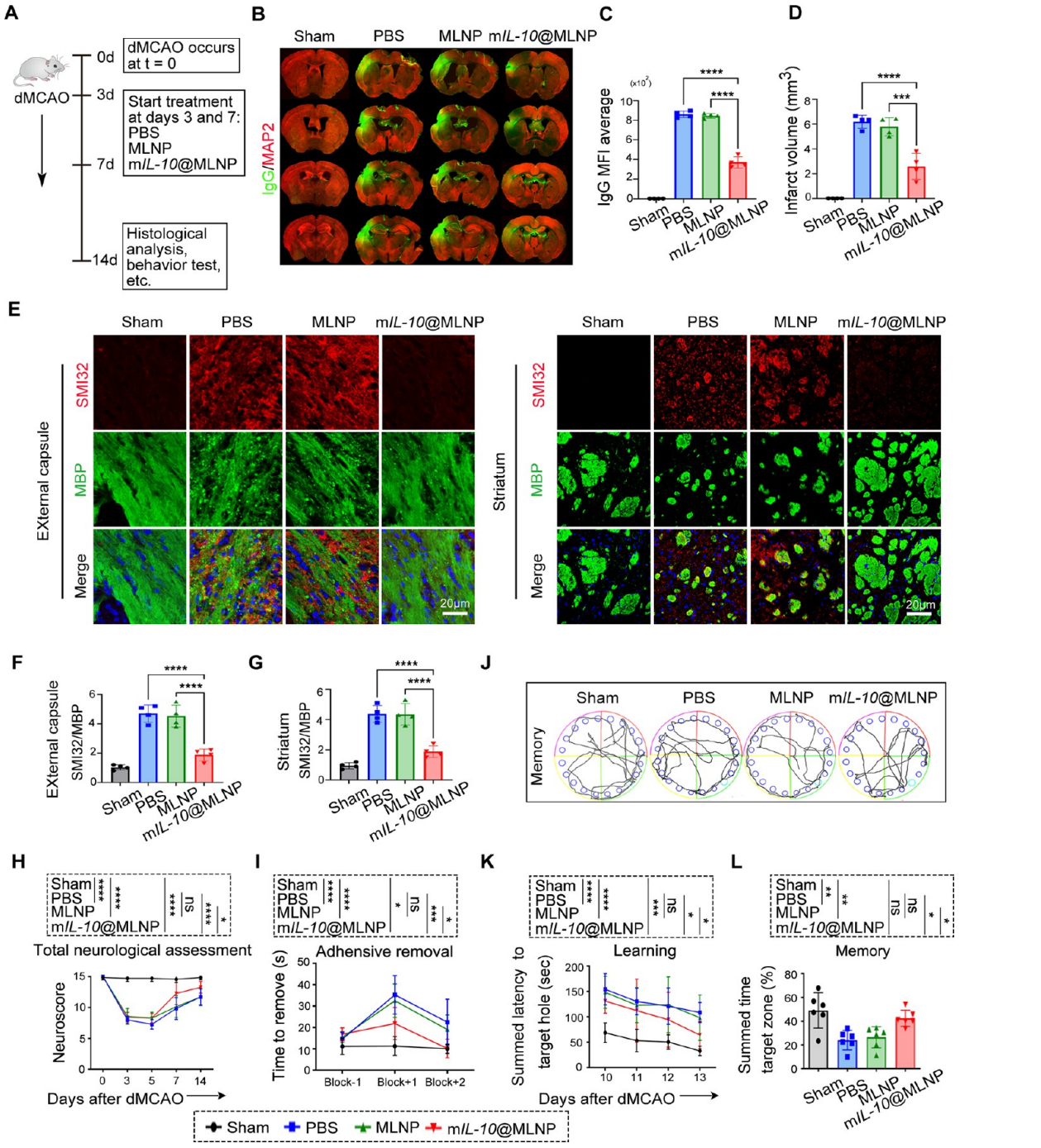

Figure 7. Therapeutic outcomes of m*IL-10*@MLNPs in a dMCAO mouse model of an ischemic stroke. (A) Schematic illustration of the treatment regimen for dMCAO mice with an established ischemic stroke. (B) Representative immunofluorescence images of endogenous IgG extravasation (green) and MAP2 (red) in brain sections obtained from sham-operated mice or dMCAO mice receiving the treatment of PBS, MLNPs, or m*IL-10*@MLNPs. (C and D) Quantitative determination of IgG leakage MFI (C) and infarct volume (D) of the indicated groups (n = 4). (E) Representative CLSM images demonstrating expression levels of SMI32 (red) and MBP (green) in the external capsule (right) and striatum (left) obtained from the indicated groups. The nuclei were labeled by using DAPI (blue). Scare bar: 20 μm. (F and G) Quantitative analysis of the SMI32/MBP MFI ratio in the external capsule (F) and striatum (G) obtained from the indicated groups (n = 4). (H) Total neurological assessment of mice in the indicated groups using the Garcia score (n = 8). (I) Evaluation of sensorimotor function in mice treated with different regimens using the adhesive removal test (n = 8). (J to L) Representative images of the moving trajectories (J) and evaluation of cognitive functions including spatial learning (K) and memory (L) ability in mice treated with different regimens using Barnes maze test (n = 6). All data are shown as means ± SD, and statistical significance was determined using one-way or two-way ANOVA (*P < 0.05, **P < 0.01, ***P < 0.001, and **** P < 0.0001). n.s., not significant.

13.38 mm^3 (MLNP control) to 34.41 ± 8.26 mm^3 (at a low dose of 0.12 mg/kg of mRNA) and 16.11 ± 0.61 mm^3 (at a high dose of 0.6 mg/kg of mRNA), respectively (Figure 5B,D).

The tight junction protein zonula occludens-1 (ZO-1) can be used as a reliable marker of endothelial barrier to reflect the pathological changes of BBB integrity.[25] ZO-1-positive

https://doi.org/10.1021/acsnano.3c09817
ACS Nano 2024, 18, 3260−3275

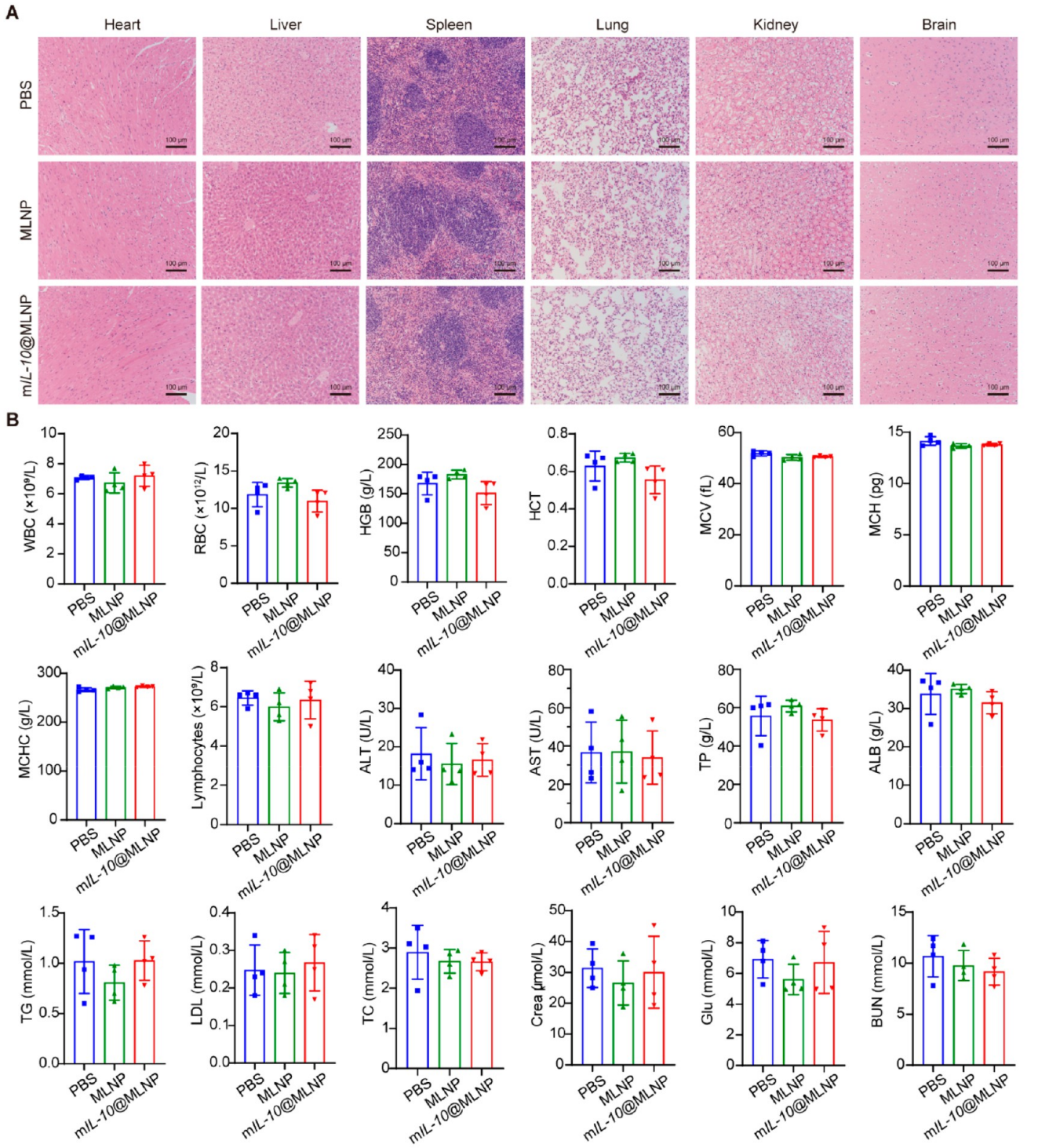

Figure 8. Safety evaluation in C57BL/6 mice. (A and B) Histological, hematological, and biochemical analysis of major organs (A) and blood samples (B) in healthy C57BL/6 mice following twice-weekly administration of m*IL-10*@MLNPs for 1 week. One week after the last injection, histological sections of organs were processed and stained with H&E for microscopic examination. Scale bars: 100 μm. The hematological and biochemical parameters analyzed in the blood samples, $n = 6$ mice per group. All data are shown as means ± SD. One-way ANOVA was performed to determine statistical significance of differences among the three groups, with no significant differences observed.

immunofluorescence staining images showed that the tight junction staining pattern was disrupted in the brain sections from tMCAO mice, revealing BBB leakage induced by an ischemia-reperfusion injury after stroke. Consistent with the IgG staining results, intravenous administration of m*IL-10*@MLNPs resulted in elevated expression of ZO-1 and restored the integrity of disrupted BBB (Figure 5E,F). Terminal deoxynucleotidyl transferase dUTP nick end labeling (TUNEL) staining was conducted to assess apoptosis in NeuN$^+$ neurons (Figure 5G,H). Results indicated that m*IL-10*@MLNP treatment significantly inhibited neuronal apoptosis after tMCAO in a dose-dependent manner. After treatment

https://doi.org/10.1021/acsnano.3c09817
ACS Nano 2024, 18, 3260−3275

with m*IL-10*@MLNP at a dosage of 0.6 mg/kg of mRNA, neuronal survival in brain sections was restored to a level comparable to that of the control group, providing additional beneficial effects in protecting against neuronal dysfunction.

m*IL-10*@MLNP Treatment Promotes M2 Polarization of Microglia and Resolves Neuroinflammation after Ischemic Stroke. To gain insight into the mechanisms underlying the therapeutic effects of m*IL-10*@MLNPs against an ischemic stroke, we tested IL-10 expression levels and microglial phenotypic shifts in tMCAO mice. The results revealed that m*IL-10*@MLNP treatment elevated IL-10 expression levels in the serum of tMCAO mice, and this expression remained detectable even 3 days post-treatment (Figure S8). Three days after m*IL-10*@MLNP administration, microglia isolated from cerebral hemispheres with ischemic lesions showed significantly increased IL-10 expression than those receiving PBS or MLNP treatment (Figure 6A,B). In parallel, there was a notable increase in the count of CD206-positive microglia observed in the cerebral ischemic hemispheres of mice treated with m*IL-10*@MLNPs than those of PBS- or blank MLNP-treated mice (Figure 6C,D). m*IL-10*@MLNPs treatment also reduced the number of cerebral $CD86^+$ microglia compared to the other two control groups (Figure 6E,F). These results indicate that successful production of bioactive IL-10 mediated by MLNPs in ischemic regions of the brain could effectively shift microglia toward M2 phenotypes, remodeling the pathological microenvironment into an anti-inflammatory state that enhances the resolution of neuroinflammation.

Next, we investigated the efficacy of m*IL-10*@MLNPs in resolving neuroinflammation by quantifying the expression of pivotal inflammation-related biomarkers in brain sections. Arg-1 is a typical hallmark of M2-polarized microglia, which greatly contributes to tissue repair and neuroprotection.[26] In contrast, TNF-α has a critical role in the neuroinflammatory response associated with multiple neurological disorders.[27] As expected, m*IL-10*@MLNPs treatment significantly elevated the cerebral expression of Arg-1 than PBS or MLNP treatment (Figure 6G,H). Observational and quantitative analyses revealed that cerebral production of TNF-α in the tMCAO mice treated with PBS or MLNPs was highly elevated after acute ischemic injury (Figure 6I,J). Strikingly, m*IL-10*@MLNP treatment resulted in a drastic reduction of TNF-α expression to levels comparable to those of the sham group, indicating the potent anti-inflammatory effects of m*IL-10*@MLNPs.

m*IL-10*@MLNP Treatment Protects against Neuronal Dysfunction in the dMCAO Mouse Model. The dMCAO model is another frequently employed an ischemic stroke model, primarily resulting in permanent cerebral cortex injury, akin to that observed in ischemic stroke patients who do not undergo recanalization therapy. The dMCAO mouse model was established to assess the effect of m*IL-10*@MLNPs on tissue injury and functional deficits caused by permanent brain ischemia. Mice were administered the indicated treatments intravenously twice, 3 and 7 days post-dMCAO procedure, respectively (Figure 7A). Brain tissues were acquired 1 week after the last injection for histological analysis. m*IL-10*@MLNPs treatment significantly reduced infarct volume and attenuated poststroke extravasation of IgG when compared to PBS or MLNP treatment (Figure 7B–D). Axonal damage and demyelination often occur in a long-time ischemic stroke, resulting in the sensorimotor and cognitive neurological dysfunction.[28,29] We first evaluated the expression of non-phosphorylated neurofilament H (SMI32), a marker of axonal loss, and myelin basic protein (MBP), a marker of myelin integrity, in external capsule and striatum sections (Figure 7E–G). Immunofluorescence staining results revealed that the external capsule and striatum sections of mice receiving PBS or M-HNP treatment had a high affinity for SMI32, and they were deficient in MBP immunoreactivity. Intriguingly, the administration of m*IL-10*@MLNPs restored the integrity of the external capsule and striatum in dMCAO mouse brains, as evidenced by the loss of SMI32 fluorescence signal and the reinstatement of MBP immunoreactivity.

Neurological deficits in mice postpermanent brain ischemia were then evaluated using multiple behavior tests, including the Garcia score, adhesive removal test, and Barnes maze. Consistent with the aforementioned immunofluorescence results, mice receiving m*IL-10*@MLNP treatment exhibited significantly higher scores in total neurological assessment up to 14 days poststroke than control groups (Figure 7H). The adhesive removal test was conducted to objectively assess the sensorimotor impairments associated with the paws and mouths of the mice. In comparison to the other two control groups, m*IL-10*@MLNP treatment group exhibited greater proficiency in sensing and removing the adhesives, as manifested by a relatively quicker response time (Figure 7I). The Barnes maze was employed to quantify the spatial cognitive abilities of dMCAO mice receiving different treatments. Intravenous administration of m*IL-10*@MLNPs significantly enhanced the spatial learning capacity of mice than PBS or blank MLNP treatment, as evidenced by the reduction in the time taken to locate a target hole that led to the escape cage (Figure 7J,K). Additionally, the mice receiving m*IL-10*@MLNP treatment spent more time in the target quadrant where they were previously trained to search for the hole, indicating an improvement in their spatial memory ability (Figure 7L). These results collectively demonstrate that M2 microglia-targeting MLNPs containing m*IL-10* exert potent neuroprotective effects by diminishing infarct volume and improving sensorimotor and cognitive function after stroke.

In Vivo Safety Evaluation. The safety of m*IL-10*@MLNPs was investigated by evaluating histological, hematological, and blood biochemical end points in healthy mice using the same dosing regimen as those for treating an ischemic stroke. Hematoxylin and eosin (H&E) staining indicated no observable signs of injury in major organs (heart, liver, spleen, lung, kidney, and brain) of mice receiving m*IL-10*@MLNP treatment (Figure 8A and Figure S9). Additionally, there were no notable differences detected in the evaluated hematological and biochemical parameters across the three treatment groups, including red blood cell count (RBC), white blood cell count (WBC), hemoglobin (HGB), hematocrit (HCT), mean corpuscular volume (MCV), mean corpuscular hemoglobin (MCH), mean corpuscular hemoglobin concentration (MCHC), lymphocytes, alanine aminotransferase (ALT), aspartate aminotransferase (AST), total protein (TP), albumin (ALB), triglycerides (TG), low-density lipoprotein (LDL), total cholesterol (TC), creatinine (Crea), urea nitrogen (BUN), or glucose (Glu) (Figure 8B and Figure S9). The evidence presented here strongly suggests that the MLNP platform is safe and nontoxic.

DISCUSSION

Microglia are widely acknowledged as the CNS resident immune cells that rapidly respond to cerebral ischemia.[30]

https://doi.org/10.1021/acsnano.3c09817
ACS Nano 2024, 18, 3260–3275

During the pathological process of an ischemic stroke, microglia play a double-edged role depending on their dynamic polarization between M2 anti-inflammatory and M1 pro-inflammatory phenotypes at different stages of injury.[31] In this context, modulating microglia polarization toward M2 phenotypes using M2-stimulating factors, such as IL-10, appears to be a promising approach for promoting repair of injured cerebral tissue and recovery of function after stroke.[8,32] Nonetheless, clinical translation of this approach is challenging due to the inherent instability of protein-based therapeutics and the potential risk of undesired immunosuppressive effects resulting from nonspecific delivery of high dose anti-inflammatory protein therapeutics.[33,34] To circumvent the limitations, we propose a targeted mRNA therapeutic strategy that induces sufficient production of bioactive IL-10 in ischemic regions of the brain to resolve neuroinflammation and treat an ischemic stroke.

The rapid authorization of LNP-based mRNA vaccines against coronavirus disease 2019 (COVID-19) highlights the transformative potential of mRNA technology.[35,36] However, the lack of delivery platforms capable of transferring mRNA therapeutics to cerebral lesion sites has hindered its translational potential for treating related brain diseases, including the ischemic stroke.[24,37] To tackle this challenge, we developed targeted MLNP platforms using the ionizable lipid AA3-Dlin that we previously reported and self-synthesized DMG-PEG-Mannose to selectively deliver m*IL-10* to brain regions of ischemic injury. Specifically, we utilize a microfluidic method to precisely formulate mRNA-loaded MLNP of ∼90 nm, which is within the optimal size range that allows the penetration of NPs across the leaky BBB and entry into the brain parenchyma following a cerebral ischemic stroke.[38,39] Upon traversing the disrupted BBB, mannose moieties can specifically recognize the CD206 receptor overexpressed on the surface of M2 microglia, thus facilitating the internalization of the developed MLNPs by M2 microglia in the brain.[40,41] AA3-Dlin components facilitate mRNA complexation and endosomal escape, contributing to the effective translation of m*IL-10* in lesional microglia in cerebral ischemic regions. Treatment with m*IL-10*@MLNPs promotes the transformation of microglia toward M2 phenotypes, resulting in increased homing of targeted MLNPs to ischemic brain lesions through CD206-mediated interactions and a consequent elevation in the production of M2-stimulating IL-10. The developed mRNA delivery strategy creates a positive feedback loop that amplifies the anti-inflammatory effects of m*IL-10* therapeutics, presenting innovative and promising clinical prospects to tackle the ischemic stroke and related neurological conditions.

The data reported here demonstrate that intravenous injection of m*IL-10*@MLNPs results in the successful colocalization of NPs with brain microglia and effective IL-10 production in the brain of tMCAO mice. This approach markedly shifts microglia toward inflammation-resolving M2 phenotypes and modulates immune response in neuro-inflammatory microenvironment by elevating the expression of trophic factors (e.g., Arg-1) and decreasing the expression of pro-inflammatory cytokines (e.g., TNF-α), ultimately restoring the disrupted BBB and inhibiting neuronal death. Notably, reduced axonal loss and improved integrity of damaged BBB and myelin were also observed when m*IL-10*@MLNPs were systemically administered 3 days after the establishment of a permanent dMCAO mouse model, suggesting an extended therapeutic time window (up to at least 72 h postonset) compared to the recanalization therapies (usually ≤24 h) currently used in clinical practice. Furthermore, m*IL-10*@MLNP treatment significantly restores sensorimotor and cognitive neurological functions in dMCAO mice, implying the neuroprotective effects of m*IL-10*@MLNPs. Hematological, blood biochemical, and histological analyses suggest that systemic administration of m*IL-10*@MLNPs is highly biocompatible, with no obvious adverse effects observed on blood biochemical indicators or the pathology of major organs.

This exploratory work mainly focuses on developing an M2 microglia-targeting mRNA-based nanotherapeutic approach to drive the polarization of brain microglia toward the M2 phenotypes poststroke and investigating its efficacy in two MCAO-induced ischemic stroke mouse models as a proof-of-concept. Our findings demonstrate that the developed mRNA nanotherapeutics can effectively resolve neuroinflammation in the ischemic brain, restore the disrupted BBB, and show great potential to extend the therapeutic time window. Targeted delivery of m*IL-10* to M2 microglia in the ischemic brain may provide a promising treatment option for a large population of stroke patients, particularly those who have failed to receive or respond to conventional treatment modalities, including intravenous thrombolysis and thrombectomy. It is noteworthy that the developed MLNP platform can be leveraged to deliver multiple RNA therapeutics (e.g., mRNA, siRNA, microRNA, or their combinations) associated with neuroimmune responses to cerebral lesion sites, offering therapeutic strategies for an ischemic stroke.

STUDY LIMITATIONS

Despite the encouraging results, additional investigations in various animal models (e.g., genetic immunodeficient mouse models) and diverse animal species (e.g., nonhuman primates) would strengthen the validation of the safety and efficacy of the targeted m*IL-10*@MLNP-based approach. The therapeutic outcomes of this strategy across different stages of acute ischemic injury and permanent brain ischemia should be further evaluated to validate its potential for translation. Delivering circular RNA encoding IL-10 and using MLNPs optimized for improved targeting capacity may hold the potential to decrease the administration frequency, minimize off-target-induced toxicity, and enhance potency and specificity. While microglia are closely involved in neuroimmune responses and play crucial roles in CNS repair, further exploration and validation are required to determine the potential application of this methodology in treating other inflammation-related brain conditions like traumatic brain injury, multiple sclerosis, and encephalitis.

CONCLUSIONS

In summary, we developed a simple and versatile mRNA delivery platform with the M2 microglia-targeting ability that allows homing of mRNA encoding phenotype-switching IL-10 to cerebral microglia in ischemic regions for poststroke tissue repair and function recovery. Intriguingly, targeted delivery of m*IL-10* elicits the effective secretion of anti-inflammatory IL-10 and enhances microglial polarization toward M2 phenotypes, which in turn augments homing of MLNPs to ischemic regions, amplifying the anti-inflammatory effects. The resulting positive feedback loop alleviates poststroke BBB disruption and restores neurological dysfunction. These findings represent a significant step forward in the develop-

https://doi.org/10.1021/acsnano.3c09817
ACS Nano 2024, 18, 3260−3275

ment of an inflammation-targeted mRNA nanotherapeutic approach, offering a promising avenue for treating an ischemic stroke and related neurological conditions. Further preclinical and clinical studies are warranted to unveil the full potential of this approach for the treatment of stroke.

EXPERIMENTAL SECTION

Materials. 1,4-Bis(2-hydroxyethyl)piperazine (amino alcohol), linoleic acid (lipid acid), 4-aminophenyl α-D-mannopyranoside (MAN), *N*,*N*-diisopropylethylamine (DIEA), and O-(7-azabenzotriazol-1-yl)-*N*,*N*,*N*′,*N*′-tetramethyluronium hexafluorophosphate (HATU) were purchased from Shanghai Aladdin Bio-Chem Technology Co., Ltd. Candida Antarctica Lipase B (CALB) and cholesterol were from Sigma-Aldrich. N_3-PEG-COOH (MW of PEG, 2000 Da) was purchased from MeloPEG. Phospholipids 1,2-dioleoyl-snglycero-3-phosphoethanolamine (DOPE) were obtained from Avanti Polar Lipids. Cy5-Cholesterol was purchased from Xi'an ruixi Biological Technology Co., Ltd. *EGFP* mRNA and Cy5-labeled mRNA were obtained from APExBIO. The immunostaining primary antibodies were as follows: anti-MAP2 (Abcam), anti-CD31 (R&D), anti-ZO-1 (Proteintech), anti-CD206 (Abcam), anti-Iba-1 (Abcam), anti-Arg-1 (Invitrogen), anti-TNF-α (Abcam), anti-NeuN (Abcam), anti-SMI32 (BioLegend), anti-MBP (Abcam), anti-GFAP (Abcam), anti-CD3 (Abcam), anti-Iba-1 (Abcam), anti-Iba-1(Wako).

Preparation of Modified *IL-10* mRNA. Templates for the mRNA transcription were acquired from murine-*IL-10* plasmids containing the 5′ and 3′ untranslated region (UTR) and 120 poly(T) (GENEWIZ). These templates underwent purification using a Universal DNA Purification and Recovery Kit (TIANGEN). All mRNAs were transcribed in vitro employing T7 RNA polymerase (Novoprotein, Shanghai, China). In this procedure, uridine-5′-triphosphate (UTP) was substituted with pseudouridine-5′-triphosphate (ΨTP; APExBIO), and antireverse cap 0 analogue (ARCA, APExBIO) was also introduced. The mRNA obtained underwent purification via RNA Clean & Concentrator (Zymo Research), quantification using NanoDrop 2000 spectrophotometer (Thermo Fisher Scientific), and was stored at −80 °C for future applications.

Synthesis of AA3-Dlin and DMG-PEG-Mannose. Synthesis of the ionizable cationic lipid AA3-Dlin was conducted as previously described.[21] Briefly, amino alcohol (0.5 g, 2.87 mmol) was mixed with a 2 molar excess of lipid acid, and the reaction was catalyzed by CALB (0.5 g) for 72 h in a nitrogen atmosphere at 60 °C. Subsequently, CALB was eliminated via centrifugation, and any surplus lipid acid was neutralized using a saturated $NaHCO_3$ solution. The compound was extracted using ethyl acetate after desiccation with anhydrous $MgSO_4$, followed by purification through rotary evaporation and vacuum drying. The obtained lipid product was characterized by liquid chromatography-mass spectrometry (Shimadzu, Japan) and ^{1}H NMR (400 MHz, Chloroform-*d*, Agilent, USA).

N_3-PEG-COOH (50 mg, 0.025 mmol) and HATU (48 mg, 0.125 mmol) were dissolved in 1.5 mL of DMF, initiating the reaction by adding DIEA (44 μL, 0.25 mmol). MAN (8.1 mg, 0.030 mmol) was incorporated into the solution and stirred at room temperature (RT) for a duration of 24 h. The resulting compound underwent a reaction with 3-(prop-2-yn-1-yloxy)propane-1,2-diyl ditetradecanoate[42] (41 mg, 0.075 mmol), utilizing a CuI (5 mg, 0.025 mmol) catalyst, maintained at RT for 24 h. The reaction was terminated by adding 50 μL of acetic acid and then diluted with methanol (5 mL). The filtered product DMG-PEG-Mannose (white solid, 5.8 mg) was purified by Prep-HPLC and characterized by ^{1}H NMR (400 MHz, Chloroform-*d*). *m*/*z* cal'd = 2842.7 ± 44.05, found 948.7 ± 14.7(1/3M+1).

Preparation of mRNA LNPs. mRNA LNPs were formulated using microfluidic devices following a previously documented procedure,[21] adjusting the molar ratio of constituents for optimization purposes. In brief, AA3-DLin, cholesterol, DOPE, and DMG-PEG-Mannose were dissolved in an ethanol phase at a molar ratio of 42.7:34.2:21.4:1.7, and mRNA was dissolved in a 25 mM sodium acetate buffer (pH 5.0) for the aqueous phase. The ethanol organic and aqueous phases were mixed using the microfluidic system (Micro&Nano, China) at a weight ratio of 20:1 between AA3-DLin and mRNA. The mixture was loaded into cassettes featuring a 3,500 MWCO (Thermo Fisher Scientific) and underwent dialysis against PBS (10 mM, pH 7.4) at 4 °C for 24 h, resulting in the formation of stable mRNA LNPs. The complete replacement of cholesterol in the formulation with Cy5-labeled cholesterol yielded Cy5-labeled LNPs for research on cellular uptake and biodistribution. The physicochemical properties, including morphologies, size, and zeta potential of mRNA LNPs was determined using TEM (Thermo Fisher Scientific, USA) and DLS (Malvern, UK).

mRNA LNPs Stability Assessment. The capacity of LNPs to protect mRNA from degradation induced by FBS was tested by agarose gel electrophoresis. In short, 1 μg of free m*IL-10*, m*IL-10*@LNPs, or m*IL-10*@MLNPs was incubated with FBS (10%, v/v) at 37 °C for up to 24 h. mRNA was extracted from LNPs using 50 mg/mL heparin sodium, analyzed by 2% agarose gel electrophoresis, and then visualized using the ChemiDoc system (Biorad, USA). mRNA LNPs were exposed in PBS supplemented with 10% FBS at 37 °C while being shaken at 100 rpm to simulate in vivo conditions. At set intervals, the particle size and aggregation states of mRNA LNPs were analyzed in triplicate with DLS and a microplate reader (Tecan, Switzerland) at 660 nm.

Isolation of Primary Microglia. Primary microglia were isolated from the postnatal C57BL/6 mouse brain. Brain tissues, excluding the cerebellum, olfactory bulbs, and meninx, were minced and digested in 0.25% Trypsin-EDTA and 125 U/mL DNase (Sigma) for 15 min at 37 °C. The brains were neutralized using complete DMEM supplemented with 10% FBS and centrifuged at 400 g for 5 min. The gathered cell pellet was resuspended in complete DMEM and cultured in a humidified incubator (5% CO2, 37 °C). After 14 days of incubation, astrocytes had achieved 100% confluency and had firmly attached to the bottom of the flask, while a subpopulation of microglia was loosely attached to the surface layer and could be detached into the culture medium by shaking the flask at 200 rpm for 4 h. To drive M2 polarization, primary microglia were exposed to 20 ng/mL of IL-4 (Peprotech) for 48 h. Subsequently, immunofluorescence was then performed to determine CD206 expression, a hallmark of M2 microglia, for differentiation characterization.

Cellular Uptake Activity. Both microglia and astrocyte were subjected to 48-h treatment with 20 ng/mL IL-4. Cells were incubated with m*IL-10*@^{Cy5}LNPs or m*IL-10*@^{Cy5}MLNPs at a concentration of 1 μg/mL mRNA for 4 h. Flow cytometry (BD Biosciences, USA) was employed for quantitative analysis of fluorescence signals, which were further observed using CLSM (Leica, Germany). M2 microglia underwent a 30 min exposure to 1 mM mannan, followed by a 4 h treatment using m*IL-10*@^{Cy5}MLNPs (1 μg/mL m*IL-10*) for 4 h, with subsequent assessment of resulting fluorescence signals through flow cytometry.

mRNA MLNPs in Vitro Transfection Activity. Microglia, at the density of 1×10^5 cells on a 24-well plate, were transfected with naked m*EGFP*, MLNPs, and m*EGFP*@M-HNPs at 1 μg/mL mRNA concentrations for 24 h. Microglia were transfected using Lipofectamine 3000 in adherence to the manufacturer's instructions, serving as a positive control. Subsequently, cell collection took place for the analysis of the MFI via flow cytometry.

Assessment of ^{Cy5}mRNA@MLNPs Endosomal Escape. Microglia, seeded at a density of 1×10^5 cells per well in confocal dishes (Costar), were incubated with ^{Cy5}mRNA@MLNPs at a 1 μg/mL mRNA concentration for 1, 2, 4, and 6 h. Cells were stained with LysoTracker Green (Beyotime) and Hoechst 33342 (Beyotime) and then imaged by CLSM.

Cytotoxicity Evaluation. Primary microglia, BV2, and bEnd.3 cells were, respectively, cultured in 96-well plates (2×10^4 cells per well) and treated with m*IL-10*@MLNPs at varying mRNA concentrations (ranging from 0.0625 to 4 μg/mL) for a duration of 24 h. The cells underwent a 2-h incubation at 37 °C with 10 μL of the CCK-8 reagents (Beyotime), followed by the measurement of absorbance at 450 nm using a microplate reader.

In Vitro Assessment of Anti-inflammatory Activity. Microglia and BV2 cells were respectively inoculated with 1×10^6 cells per well

https://doi.org/10.1021/acsnano.3c09817
ACS Nano 2024, 18, 3260−3275

in 6-well plates. Cells initially underwent a 4 h stimulation of 500 ng/mL LPS, then subjected to incubation for 24 h with either fresh medium or m*IL-10*@MLNPs (1 μg/mL). The total RNA was extracted using Trizol and RT-qPCR was employed to measure the gene levels of *IL-10*, *TNF-α*, *iNOS*, *IL-6*, *Arg-1*, *TGF-β*, or *CD206*. Primers for each gene are listed in Table S2. The supernatant was gathered to measure IL-10, TNF-α, and TGF-β levels employing ELISA kits for quantification (NeoBioscience Technology Co, Ltd.). Proteins obtained from the cells via RIPA lysis buffer were assessed for Arg-1 (anti-Arg-1, Servicebio) and CD206 (anti-CD206, Proteintech) protein levels using a Western blotting assay.

Animals. The procedures received approval from the Renji Hospital Institutional or Shanghai Jiao Tong University Animal Care and Use Committee and were conducted following the Institutional Guide for the Care and Use of Laboratory Animals. Male C57/BL6 mice (8−10 weeks old) were procured from Shanghai SLAC Laboratory Animals. Randomization and allocation concealment were conducted. Briefly, mice were labeled using the animal facility labeling system and randomly assigned to the experimental groups. Investigators conducted surgeries and outcome assessments without knowledge of the experimental group assignments, ensuring blindness throughout the process.

Murine Focal Cerebral Ischemia Models. Male C57/BL6 mice (8−10 weeks old) underwent tMCAO following established procedures.[43] Concisely, a monofilament was threaded via the common carotid artery of mice to reach the middle cerebral artery origin, remaining in place for 60 min before removal and triggering reperfusion. During surgical procedures, a heating pad maintained body temperature at 37 ± 0.5 °C, while a laser Doppler flowmeter (PERIMED-PeriCam PSI, Sweden) measured cerebral blood flow, confirming both vascular occlusion and reperfusion. After undergoing MCAO surgery, mice failing to show a decrease in the regional cerebral blood flow to 30% of their preischemia baseline levels were discarded. Mice in the sham-operated group received identical anesthesia and surgical incision, excluding middle cerebral artery occlusion. Mice were administrated with PBS, Naked m*IL-10*, mNc@MLNPs, MLNPs, and m*IL-10*@MLNPs 2 h post-tMCAO at a dose of 0.12 or 0.6 mg/kg mRNA per mouse and were sacrificed 3 days later to evaluate the therapeutic effects.

To induce dMCAO, the initial steps involved a neck incision to expose and ligate the left common carotid artery. Following suturing of the neck incision, a subsequent incision was performed between the eye and ear. Dissection of the temporal muscle and creation of a burr hole revealed the distal part. Subsequently, an incision was made in the dura mater, and low-intensity bipolar electrocautery (Shanghai Hutong Electronics Co. Ltd.) was applied at the immediate lateral section of the rhinal fissure to coagulate the dMCAO. Mice in the sham-operated group received identical anesthesia and arterial surgical exposure, but without the occlusion of arteries. Mice were administrated with PBS, MLNPs, and m*IL-10*@MLNPs at a dose of 0.3 mg/kg mRNA per mouse 3 and 7 days post-dMCAO, and were sacrificed 7 days after the last injection to evaluate the therapeutic outcomes. Mice were sacrificed by high CO_2 asphyxiation, with the number of animals receiving surgery determined based on prior experimentation in our lab to minimize animal suffering and the usage of animals.

Biodistribution of Cy5-Labeled LNPs in tMCAO Mice. tMCAO mice were intravenously injected with m*IL-10*@^{Cy5}LNPs or m*IL-10*@^{Cy5}MLNP (0.6 mg/kg of mRNA per mouse). Twenty-four hours later, the mice underwent anesthesia, followed by perfused with PBS containing 4% paraformaldehyde. Subsequently, IVIS (PerkinElmer, USA) was utilized to capture images of the brain and other vital organs (heart, spleen, liver, kidney, and lung). The fluorescence intensity was quantitively analyzed by Living Image 4.5 software.

ELISA Assay. The serum and brain tissues were harvested from the tMCAO mice following the indicated treatments. Brain tissues were homogenized in saline and then centrifuged. The IL-10 levels in the supernatant of brain tissues and serum were quantified using ELISA kits (NeoBioscience Technology Co, Ltd.).

Immunofluorescence Staining. After a 30 min block with 3% BSA, the sections underwent an overnight incubation at 4 °C with the primary antibody. Subsequently, they underwent a 60 min incubation with appropriate fluorescent-labeled secondary antibodies, followed by a 5 min counterstain with DAPI at RT. Histological images were acquired either through CLSM (Olympus Fluoview FV3000, Olympus, Center Valley PA) or a microscope (Olympus) and were quantitatively analyzed using ImageJ software. The average percentage per field within sections represented the count of immuno-positive cells. Investigators blinded to the study randomly selected fields within three consecutive sections per brain cortex for analysis.

TUNEL Staining. The analysis of apoptotic cells was conducted utilizing the TUNEL kit, following well-established protocols.[44] The sections underwent a 1 h incubation with the TUNEL kit (Roche) within a humidified chamber at 37 °C. Double-label immunofluorescence for NeuN (anti-NeuN, Abcam) and TUNEL was imaged via CLSM.

Flow Cytometry. Following the manufacturer's instructions, the cerebral hemispheres from mice subjected to either tMCAO or sham operations were mixed with Neural Tissue Dissociation reagent (130-093-231, Miltenyi Biotec) and homogenized via the gentle MACS Dissociator (Miltenyi Biotec, Germany). Antibodies specific for microglial surface markers (anti-CD45-PE-Cy7, Invitrogen; anti-CD11b-FITC, BD), an M2 phenotypic marker (anti-CD206-APC, Invitrogen), an M1 phenotypic marker (anti-CD86-BV510, BD), and an anti-IL-10-bv421 (BD) were used in flow cytometry to characterize immune cells. Data was analyzed using FlowJo software (TreeStar).

Evaluation of Neurological Function. The sensorimotor functions of mice before and after surgery were evaluated using the modified Garcia Score[45,46] and Adhesive Test.[47] The modified Garcia Score encompasses five distinct tests: proprioception, forelimb walking, lateral turning, limb symmetry, and climbing. Among these, one evaluates sensor function, while the remaining four appraise motor function. Each test yields a score from 0 to 3, contributing to a maximum score of 15.

During the adhesive removal test, adhesive tapes sized at 0.3 cm × 0.4 cm were randomly affixed to each paw of the mice, and the duration taken for the mice to remove each tape was noted. Before the procedure, mice received 3 days of once daily training and then underwent scheduled poststroke tests. At specified times, each day involved three tests per mouse, with 15 min intervals between tests. The average latency in touching and removing the tapes was calculated across 3 trials for each mouse.

Barnes Maze. The Barnes maze test slightly refined using insights from prior research.[48] In essence, the maze was composed of a white PVC circular slab (36 in. in diameter, 8 mm thick). The circular platform featured 20 holes, each 3 in. in diameter, located 1 in. from the edge. It sited atop a rotating stool, elevated to a height of 30 in. from the ground. The escape cages, made from mouse cages coated in black tape to prevent light ingress, were situated on a platform positioned 2 in. below the maze surface and linked to the maze through a ramp. The maze was centrally located within a dedicated room flanked by 120 W lights on each side, providing aversive stimuli for the mice. Visual cues in the form of eight colored-paper shapes (rectangles, squares, and circles) adorned the room's walls. After each mouse's test, any intragaze odor or visual cues were eliminated by cleaning with 70% ethanol and rotating the maze clockwise. SMART 3.0 video tracking software was used to record all sessions.

The Barnes maze test comprises three stages: habituation on day 1, training from days 2 to 5, and probe on day 6. Before each experiment, mice underwent a 1 h acclimation period in the testing room. Then, all mice were housed individually in separate cages until the daily testing was completed. During the habituation phase, the mice were positioned at the maze's center, where they encountered a vertically oriented black PVC pipe measuring 7 in. height and 4 in. diameter, remaining there for a duration of 15 s. The mice were gently directed toward the escape cage's entrance over 10−15 s. Subsequently, they were granted 3 min to enter the target hole unaided; if needed, gentle nudges with the PVC pipe were provided

https://doi.org/10.1021/acsnano.3c09817
ACS Nano 2024, 18, 3260−3275

for assistance. Afterward, the 120 W lights were turned off, the mice had a 2 min rest period inside the escape cage.

The training phase, which followed the habituation phase by 24 h, spanned 4 days. It consisted of 3 trials on the initial day and 4 trials on each of the subsequent 3 days. In every trial, the mice spent 15 s within the PVC pipe at the maze center before a 3 min exploration period commenced. If they reached the target hole before the 3 min lapsed, the trial ended with the lights off. A subsequent 2 min rest period was granted in the escape cage. In case the mice had not entered the target hole within the time frame, they received nudges with the PVC pipe. Both the time taken to enter the target hole and the distance traveled in each trial were recorded.

The probe phase (day 6), scheduled 24 h after the training phase, involved placing mice within the maze center using the PVC pipe for 15 s, followed by a 2 min exploration period. This phase focused on recording the time spent in each quadrant, the latency to reach the target hole, and the distance traveled by the mice.

Safety Evaluation. Male C56BL/6 mice were injected with PBS, MLNPs, or m*IL-10*@MLNPs according to dosing regimens similar to those used in pharmacodynamic experiments, with administration once at 0.6 mg/kg mRNA per mouse or twice weekly for 1 week at a dose of 0.3 mg/kg mRNA per mouse. Three or 7 days after the final injection, blood and major organ samples were collected from each treatment group. Histological assessments using H&E staining were performed on the hearts, livers, spleens, lungs, kidneys, and brains. Simultaneously, blood samples underwent analysis for hematological and biochemical indicators.

Statistical Analysis. To determine normality, Shapiro–Wilk and Kolmogorov–Smirnov normality tests were utilized. One-way analysis of variance was employed for comparing multiple groups in cases of normal distribution. For non-normally distributed data, *P* values were computed using Kruskal–Wall's test. To analyze differences among various groups at different time points, two-way ANOVAs were conducted, followed by the Bonferroni post hoc test. A significance level of $P < 0.05$ was considered statistically significant. Graphs display statistical significance as follows: $^{*}P < 0.05$, $^{**}P < 0.01$, $^{***}P < 0.001$, and $^{****}P < 0.0001$. Statistical analyses were performed using GraphPad Prism 8 software, version v8.2.1.

ASSOCIATED CONTENT

Supporting Information

The Supporting Information is available free of charge at https://pubs.acs.org/doi/10.1021/acsnano.3c09817.

Figures S1–S3: The characterization of AA3-DLin and DMG-PEG-Mannose by mass spectrometry and ^{1}H NMR spectrum. Figures S4–S6: The uptake, biodistribution, and cytotoxicity evaluation of LNPs. Figure S7: mRNA expression of inflammatory cytokines in cells with indicated treatments. Figure S8: Serum levels of IL-10 in tMCAO mice receiving treatment of m*IL-10*@MLNPs. Figure S9: Safety evaluation of LNPs in healthy mice. Table S1: m*IL-10* sequences utilized in this study. Table S2: Primer sequences of RT-qPCR. (PDF)

AUTHOR INFORMATION

Corresponding Authors

Peiying Li – *Department of Anesthesiology, Renji Hospital and Clinical Research Center, Renji Hospital, Shanghai Jiao Tong University School of Medicine, Shanghai 200127, China; Key Laboratory of Anesthesiology (Shanghai Jiao Tong University), Ministry of Education, Shanghai 200127, China*; Email: peiyingli.md@gmail.com

Xue-Qing Zhang – *Shanghai Frontiers Science Center of Drug Target Identification and Delivery, School of Pharmaceutical Sciences, Shanghai Jiao Tong University, Shanghai 200240, China; National Key Laboratory of Innovative Immunotherapy (Shanghai Jiao Tong University), Shanghai 200240, China*; orcid.org/0000-0002-4954-2586; Email: xueqingzhang@sjtu.edu.cn

Authors

Mingzhu Gao – *Shanghai Frontiers Science Center of Drug Target Identification and Delivery, School of Pharmaceutical Sciences, Shanghai Jiao Tong University, Shanghai 200240, China; National Key Laboratory of Innovative Immunotherapy (Shanghai Jiao Tong University), Shanghai 200240, China*

Yan Li – *Department of Anesthesiology, Renji Hospital, Shanghai Jiao Tong University School of Medicine, Shanghai 200127, China; Key Laboratory of Anesthesiology (Shanghai Jiao Tong University), Ministry of Education, Shanghai 200127, China*

William Ho – *Department of Chemical and Materials Engineering, New Jersey Institute of Technology, Newark, New Jersey 07102, United States*

Chen Chen – *Department of Anesthesiology, Renji Hospital, Shanghai Jiao Tong University School of Medicine, Shanghai 200127, China; Key Laboratory of Anesthesiology (Shanghai Jiao Tong University), Ministry of Education, Shanghai 200127, China*

Qijing Chen – *Shanghai Frontiers Science Center of Drug Target Identification and Delivery, School of Pharmaceutical Sciences, Shanghai Jiao Tong University, Shanghai 200240, China; National Key Laboratory of Innovative Immunotherapy (Shanghai Jiao Tong University), Shanghai 200240, China*

Fengshi Li – *Key Laboratory of Anesthesiology (Shanghai Jiao Tong University), Ministry of Education, Shanghai 200127, China; Department of Neurosurgery, Center of Cerebrovascular Disease, Renji Hospital, Shanghai Jiao Tong University School of Medicine, Shanghai 200127, China*

Maoping Tang – *Shanghai Frontiers Science Center of Drug Target Identification and Delivery, School of Pharmaceutical Sciences, Shanghai Jiao Tong University, Shanghai 200240, China; National Key Laboratory of Innovative Immunotherapy (Shanghai Jiao Tong University), Shanghai 200240, China*

Qiuyue Fan – *Department of Anesthesiology, Renji Hospital, Shanghai Jiao Tong University School of Medicine, Shanghai 200127, China; Key Laboratory of Anesthesiology (Shanghai Jiao Tong University), Ministry of Education, Shanghai 200127, China*

Jieqing Wan – *Key Laboratory of Anesthesiology (Shanghai Jiao Tong University), Ministry of Education, Shanghai 200127, China; Department of Neurosurgery, Center of Cerebrovascular Disease, Renji Hospital, Shanghai Jiao Tong University School of Medicine, Shanghai 200127, China*

Weifeng Yu – *Department of Anesthesiology, Renji Hospital, Shanghai Jiao Tong University School of Medicine, Shanghai 200127, China; Key Laboratory of Anesthesiology (Shanghai Jiao Tong University), Ministry of Education, Shanghai 200127, China*

Xiaoyang Xu – *Department of Chemical and Materials Engineering, New Jersey Institute of Technology, Newark, New Jersey 07102, United States; Department of Biomedical Engineering, New Jersey Institute of Technology, Newark, New Jersey 07102, United States*; orcid.org/0000-0002-1634-3329

Complete contact information is available at:

https://pubs.acs.org/10.1021/acsnano.3c09817

Author Contributions

M.G. and Y.L. contributed equally to this work. Conceptualization: X.-Q.Z., P.L., X.X., M.G., and Y.L. Methodology: X.-Q.Z., P.L., M.G., Y.L., W.H., C.C., Q.C., F.L., M.T., Q.F., J.W., and W.Y. Investigation: M.G., Y.L., W.H., C.C., Q.C., F.L., M.T., Q.F., J.W., and W.Y. Visualization: M.G. and Y.L. Supervision: X.-Q.Z., P.L., and X.X. Writing-original draft: X.-Q.Z., M.G., and Y.L. Writing-review and editing: X.-Q.Z., P.L., X.X., and M.G.

Notes

The authors declare no competing financial interest.

ACKNOWLEDGMENTS

X.-Q.Z. acknowledges funding from the National Key Research and Development Program of China (2023YFC2606003), "Open Competition to Select the Best Candidates" Key Technology Program for Nucleic Acid Drugs of NCTIB (Grant No. NCTIB2022HS02002), Natural Science Foundation of Shanghai (23ZR1427600), and Shanghai Jiao Tong University Scientific and Technological Innovation Funds (2019TPA10). P.L. is supported by the National Natural Science Foundation of China (NSFC, 91957111, 81971096, 82061130224, M-0671, U22A20295), New Frontier Technology Joint Research (SHDC12019102) and Ward Building Project for Demonstration and Research sponsored by Shanghai Shenkang Hospital Development Center, Shanghai Municipal Education Commission-Gaofeng Clinical Medical Grant Support (20181805), "Shuguang Program" supported by Shanghai Education Development Foundation and Shanghai Municipal Education Commission (20SG17), "Shanghai Outstanding Academic Leaders Program" from Shanghai Municipal Science and Technology Committee (20XD1422400), the Newton Advanced Fellowship grant provided by the UK Academy of Medical Sciences (NAF \R11\1010) and the Innovative Research Team of High-level Local Universities in Shanghai (SHSMU-ZLCX20211602), Shanghai Engineering Research Center of Peri-operative Organ Support and Function Preservation (20DZ2254200).

REFERENCES

(1) Qin, C.; Yang, S.; Chu, Y.-H.; Zhang, H.; Pang, X.-W.; Chen, L.; Zhou, L.-Q.; Chen, M.; Tian, D.-S.; Wang, W. Signaling pathways involved in ischemic stroke: molecular mechanisms and therapeutic interventions. *Signal Transduction and Targeted Therapy* **2022**, *7* (1), 215.

(2) Tsao, C. W.; Aday, A. W.; Almarzooq, Z. I.; Anderson, C. A.; Arora, P.; Avery, C. L.; Baker-Smith, C. M.; Beaton, A. Z.; Boehme, A. K.; Buxton, A. E. Heart disease and stroke statistics—2023 update: a report from the American Heart Association. *Circulation* **2023**, *147* (8), e93−e621.

(3) Campbell, B. C. V.; De Silva, D. A.; Macleod, M. R.; Coutts, S. B.; Schwamm, L. H.; Davis, S. M.; Donnan, G. A. Ischaemic stroke. *Nature Reviews Disease Primers* **2019**, *5* (1), 70.

(4) Iadecola, C.; Anrather, J. The immunology of stroke: from mechanisms to translation. *Nature Medicine* **2011**, *17* (7), 796−808.

(5) Candelario-Jalil, E.; Dijkhuizen, R. M.; Magnus, T. Neuroinflammation, Stroke, Blood-Brain Barrier Dysfunction, and Imaging Modalities. *Stroke* **2022**, *53* (5), 1473−1486.

(6) Nadareishvili, Z.; Simpkins, A. N.; Hitomi, E.; Reyes, D.; Leigh, R. Post-Stroke Blood-Brain Barrier Disruption and Poor Functional Outcome in Patients Receiving Thrombolytic Therapy. *Cerebrovasc Dis* **2019**, *47* (3−4), 135−142.

(7) Fu, Y.; Liu, Q.; Anrather, J.; Shi, F.-D. Immune interventions in stroke. *Nature Reviews Neurology* **2015**, *11* (9), 524−535.

(8) Hu, X.; Leak, R. K.; Shi, Y.; Suenaga, J.; Gao, Y.; Zheng, P.; Chen, J. Microglial and macrophage polarization—new prospects for brain repair. *Nature Reviews Neurology* **2015**, *11* (1), 56−64.

(9) Orihuela, R.; McPherson, C. A.; Harry, G. J. Microglial M1/M2 polarization and metabolic states. *Br. J. Pharmacol.* **2016**, *173* (4), 649−665.

(10) Guo, Y.; Dai, W.; Zheng, Y.; Qiao, W.; Chen, W.; Peng, L.; Zhou, H.; Zhao, T.; Liu, H.; Zheng, F. Mechanism and Regulation of Microglia Polarization in Intracerebral Hemorrhage. *Molecules* **2022**, *27* (20), 7080.

(11) Tu, Z.; Zhong, Y.; Hu, H.; Shao, D.; Haag, R.; Schirner, M.; Lee, J.; Sullenger, B.; Leong, K. W. Design of therapeutic biomaterials to control inflammation. *Nat. Rev. Mater.* **2022**, *7* (7), 557−574.

(12) Lyu, J.; Xie, D.; Bhatia, T. N.; Leak, R. K.; Hu, X.; Jiang, X. Microglial/Macrophage polarization and function in brain injury and repair after stroke. *CNS Neurosci Ther* **2021**, *27* (5), 515−527.

(13) Mattos, A.; de Jager-Krikken, A.; de Haan, M.; Beljaars, L.; Poelstra, K. PEGylation of interleukin-10 improves the pharmacokinetic profile and enhances the antifibrotic effectivity in CCl_4-induced fibrogenesis in mice. *J. Controlled Release* **2012**, *162* (1), 84−91.

(14) Donohue, J. H.; Rosenberg, S. A. The fate of interleukin-2 after in vivo administration. *J. Immunol* **1983**, *130* (5), 2203−2208.

(15) Huang, X.; Kong, N.; Zhang, X.; Cao, Y.; Langer, R.; Tao, W. The landscape of mRNA nanomedicine. *Nat. Med.* **2022**, *28* (11), 2273−2287.

(16) Wei, T.; Cheng, Q.; Farbiak, L.; Anderson, D. G.; Langer, R.; Siegwart, D. J. Delivery of Tissue-Targeted Scalpels: Opportunities and Challenges for In Vivo CRISPR/Cas-Based Genome Editing. *ACS Nano* **2020**, *14* (8), 9243−9262.

(17) Xiao, Y.; Chen, J.; Zhou, H.; Zeng, X.; Ruan, Z.; Pu, Z.; Jiang, X.; Matsui, A.; Zhu, L.; Amoozgar, Z.; et al. Combining p53 mRNA nanotherapy with immune checkpoint blockade reprograms the immune microenvironment for effective cancer therapy. *Nat. Commun.* **2022**, *13* (1), 758.

(18) Rohner, E.; Yang, R.; Foo, K. S.; Goedel, A.; Chien, K. R. Unlocking the promise of mRNA therapeutics. *Nat. Biotechnol.* **2022**, *40* (11), 1586−1600.

(19) Rurik, J. G.; Tombácz, I.; Yadegari, A.; Méndez Fernández, P. O.; Shewale, S. V.; Li, L.; Kimura, T.; Soliman, O. Y.; Papp, T. E.; Tam, Y. K.; et al. CAR T cells produced in vivo to treat cardiac injury. *Science* **2022**, *375* (6576), 91−96.

(20) Xu, X.; Xie, K.; Zhang, X. Q.; Pridgen, E. M.; Park, G. Y.; Cui, D. S.; Shi, J.; Wu, J.; Kantoff, P. W.; Lippard, S. J.; et al. Enhancing tumor cell response to chemotherapy through nanoparticle-mediated codelivery of siRNA and cisplatin prodrug. *Proc. Natl. Acad. Sci. U. S. A.* **2013**, *110* (46), 18638−18643.

(21) Li, Z.; Zhang, X. Q.; Ho, W.; Li, F.; Gao, M.; Bai, X.; Xu, X. Enzyme-Catalyzed One-Step Synthesis of Ionizable Cationic Lipids for Lipid Nanoparticle-Based mRNA COVID-19 Vaccines. *ACS Nano* **2022**, *16* (11), 18936−18950.

(22) Corbett, K. S.; Edwards, D. K.; Leist, S. R.; Abiona, O. M.; Boyoglu-Barnum, S.; Gillespie, R. A.; Himansu, S.; Schäfer, A.; Ziwawo, C. T.; DiPiazza, A. T.; et al. SARS-CoV-2 mRNA vaccine design enabled by prototype pathogen preparedness. *Nature* **2020**, *586* (7830), 567−571.

(23) Poon, W.; Kingston, B. R.; Ouyang, B.; Ngo, W.; Chan, W. C. W. A framework for designing delivery systems. *Nat. Nanotechnol* **2020**, *15* (10), 819−829.

(24) Lu, Z.-G.; Shen, J.; Yang, J.; Wang, J.-W.; Zhao, R.-C.; Zhang, T.-L.; Guo, J.; Zhang, X. Nucleic acid drug vectors for diagnosis and treatment of brain diseases. *Signal Transduction and Targeted Therapy* **2023**, *8* (1), 39.

(25) Zhang, W.; Zhu, L.; An, C.; Wang, R.; Yang, L.; Yu, W.; Li, P.; Gao, Y. The blood brain barrier in cerebral ischemic injury - Disruption and repair. *Brain Hemorrhages* **2020**, *1* (1), 34−53.

(26) Cherry, J. D.; Olschowka, J. A.; O'Banion, M. K. Neuroinflammation and M2 microglia: the good, the bad, and the inflamed. *J. Neuroinflammation* **2014**, *11*, 98.
(27) Mishra, A.; Bandopadhyay, R.; Singh, P. K.; Mishra, P. S.; Sharma, N.; Khurana, N. Neuroinflammation in neurological disorders: pharmacotherapeutic targets from bench to bedside. *Metabolic Brain Disease* **2021**, *36* (7), 1591−1626.
(28) Shi, H.; Hu, X.; Leak, R. K.; Shi, Y.; An, C.; Suenaga, J.; Chen, J.; Gao, Y. Demyelination as a rational therapeutic target for ischemic or traumatic brain injury. *Exp. Neurol.* **2015**, *272*, 17−25.
(29) Shi, L.; Sun, Z.; Su, W.; Xu, F.; Xie, D.; Zhang, Q.; Dai, X.; Iyer, K.; Hitchens, T. K.; Foley, L. M.; et al. Treg cell-derived osteopontin promotes microglia-mediated white matter repair after ischemic stroke. *Immunity* **2021**, *54* (7), 1527−1542.e1528.
(30) Shichita, T.; Ooboshi, H.; Yoshimura, A. Neuroimmune mechanisms and therapies mediating post-ischaemic brain injury and repair. *Nat. Rev. Neurosci.* **2023**, *24* (5), 299−312.
(31) Zhao, S.-c.; Ma, L.-s.; Chu, Z.-h.; Xu, H.; Wu, W.-q.; Liu, F. Regulation of microglial activation in stroke. *Acta Pharmacologica Sinica* **2017**, *38* (4), 445−458.
(32) Zhu, H.; Hu, S.; Li, Y.; Sun, Y.; Xiong, X.; Hu, X.; Chen, J.; Qiu, S. Interleukins and Ischemic Stroke. *Front Immunol* **2022**, *13*, 828447.
(33) Sathish, J. G.; Sethu, S.; Bielsky, M. C.; de Haan, L.; French, N. S.; Govindappa, K.; Green, J.; Griffiths, C. E.; Holgate, S.; Jones, D.; et al. Challenges and approaches for the development of safer immunomodulatory biologics. *Nat. Rev. Drug Discov* **2013**, *12* (4), 306−324.
(34) Minshawi, F.; Lanvermann, S.; McKenzie, E.; Jeffery, R.; Couper, K.; Papoutsopoulou, S.; Roers, A.; Muller, W. The Generation of an Engineered Interleukin-10 Protein With Improved Stability and Biological Function. *Front Immunol* **2020**, *11*, 1794.
(35) Chaudhary, N.; Weissman, D.; Whitehead, K. A. mRNA vaccines for infectious diseases: principles, delivery and clinical translation. *Nat. Rev. Drug Discov* **2021**, *20* (11), 817−838.
(36) Kowalski, P. S.; Rudra, A.; Miao, L.; Anderson, D. G. Delivering the Messenger: Advances in Technologies for Therapeutic mRNA Delivery. *Mol. Ther* **2019**, *27* (4), 710−728.
(37) Paunovska, K.; Loughrey, D.; Dahlman, J. E. Drug delivery systems for RNA therapeutics. *Nat. Rev. Genet.* **2022**, *23* (5), 265−280.
(38) Mitchell, M. J.; Billingsley, M. M.; Haley, R. M.; Wechsler, M. E.; Peppas, N. A.; Langer, R. Engineering precision nanoparticles for drug delivery. *Nat. Rev. Drug Discovery* **2021**, *20* (2), 101−124.
(39) Sethi, B.; Kumar, V.; Mahato, K.; Coulter, D. W.; Mahato, R. I. Recent advances in drug delivery and targeting to the brain. *J. Controlled Release* **2022**, *350*, 668−687.
(40) Zimmer, H.; Riese, S.; Régnier-Vigouroux, A. Functional characterization of mannose receptor expressed by immunocompetent mouse microglia. *Glia* **2003**, *42* (1), 89−100.
(41) Ganbold, T.; Bao, Q.; Zandan, J.; Hasi, A.; Baigude, H. Modulation of Microglia Polarization through Silencing of NF-κB p65 by Functionalized Curdlan Nanoparticle-Mediated RNAi. *ACS Appl. Mater. Interfaces* **2020**, *12* (10), 11363−11374.
(42) Reise, F.; Warias, J. E.; Chatterjee, K.; Krekiehn, N. R.; Magnussen, O.; Murphy, B. M.; Lindhorst, T. K. Photoswitchable Glycolipid Mimetics: Synthesis and Photochromic Properties of Glycoazobenzene Amphiphiles. *Chemistry* **2018**, *24* (66), 17497−17505.
(43) Mracsko, E.; Liesz, A.; Stojanovic, A.; Lou, W. P.; Osswald, M.; Zhou, W.; Karcher, S.; Winkler, F.; Martin-Villalba, A.; Cerwenka, A.; et al. Antigen dependently activated cluster of differentiation 8-positive T cells cause perforin-mediated neurotoxicity in experimental stroke. *J. Neurosci.* **2014**, *34* (50), 16784−16795.
(44) Leak, R. K.; Zhang, L.; Stetler, R. A.; Weng, Z.; Li, P.; Atkins, G. B.; Gao, Y.; Chen, J. HSP27 protects the blood-brain barrier against ischemia-induced loss of integrity. *CNS Neurol Disord Drug Targets* **2013**, *12* (3), 325−337.
(45) Cekanaviciute, E.; Fathali, N.; Doyle, K. P.; Williams, A. M.; Han, J.; Buckwalter, M. S. Astrocytic transforming growth factor-beta signaling reduces subacute neuroinflammation after stroke in mice. *Glia* **2014**, *62* (8), 1227−1240.
(46) Doyle, K. P.; Fathali, N.; Siddiqui, M. R.; Buckwalter, M. S. Distal hypoxic stroke: a new mouse model of stroke with high throughput, low variability and a quantifiable functional deficit. *J. Neurosci Methods* **2012**, *207* (1), 31−40.
(47) Bouet, V.; Boulouard, M.; Toutain, J.; Divoux, D.; Bernaudin, M.; Schumann-Bard, P.; Freret, T. The adhesive removal test: a sensitive method to assess sensorimotor deficits in mice. *Nat. Protoc* **2009**, *4* (10), 1560−1564.
(48) Minhas, P. S.; Latif-Hernandez, A.; McReynolds, M. R.; Durairaj, A. S.; Wang, Q.; Rubin, A.; Joshi, A. U.; He, J. Q.; Gauba, E.; Liu, L.; et al. Restoring metabolism of myeloid cells reverses cognitive decline in ageing. *Nature* **2021**, *590* (7844), 122−128.

https://doi.org/10.1021/acsnano.3c09817
ACS Nano 2024, 18, 3260−3275